Review

Structure optimization of ruthenium photosensitizers for efficient dye-sensitized solar cells – A goal toward a "bright" future

Jen-Fu Yin [a,b], Murugesan Velayudham [a], Dibyendu Bhattacharya [a], Hong-Cheu Lin [b], Kuang-Lieh Lu [a,*]

[a] Institute of Chemistry, Academia Sinica, Taipei 115, Taiwan
[b] Department of Materials Science and Engineering, National Chiao Tung University, Hsinchu 300, Taiwan

Contents

ARTICLE INFO

ABSTRACT

Research on dye-sensitized solar cells (DSC) is progressing at a rapid pace. The structural and electronic factors associated with ruthenium photosensitizers can have a significant effect on the performance of DSCs. This review emphasizes the recent developments and strategies employed in the structural design of ruthenium photosensitizers. The influence of molecular engineering on photophysical and electrochemical properties along with photovoltaic parameters and the efficiency of DSCs are also reviewed. Hence, drawing a correlation between the structure of photosensitizers, the properties and photovoltaic parameters of corresponding DSCs will be helpful in terms of optimizing new dyes for the generation of efficient solar cells.

© 2012 Elsevier B.V. All rights reserved.

1. Introduction

The energy crisis is one of the challenging problems confronting mankind today. According to International Energy Outlook (IEO) 2010, the total world energy use is predicted to rise from 14.8 TW in 2008 to 18.2 TW in 2020 and to reach 22.6 TW in 2035 [1]. Hoffert et al. projected that world energy consumption rate will double from 13.7 TW in 2001 to 27 TW by 2050 and will triple to 43 TW by 2100 [2]. With the immense use of oil and coal as fuels, an enormous amount of CO_2 is released into the atmosphere, which is thought to be the main contributor to global warming. To reduce CO_2 emissions, new avenues are being explored for generating carbon-emission-free power. Furthermore, the resources of coal, oil and natural gas are dwindling rapidly, which is a source of stimulation in terms of considering alternative energy sources [3]. Non-conventional energy sources such as, solar energy and wind energy are known to be low-carbon emitting energy sources [4]. It is projected that the contribution from renewable energy sources will occupy a prominent place in the future [5]. In particular, solar energy has tremendous potential, because it is available all around the globe, and is inexhaustible and environmentally benign [6].

The solar energy incident on the earth's surface, whose globally convertible power is estimated to be 120,000 TW, is sufficient to satisfy the world's requirements [7]. Therefore, the practical and efficient use of solar energy has been a consistently significant topic in the world [6].

Because of the inherently expensive cost of manufacturing, the price of silica-based solar cells is very high and hence dye-sensitized solar cells (DSC) promise to be a viable alternative owing to their low cost, flexibility and various colors. Furthermore, DSCs display higher efficiencies at low light levels and the angle of the incident light has no great effect on performance. The new technology concerning the DSCs, where light absorption occurs by dye molecules attached to a nanostructured semiconductor oxide material, is steadily growing [8]. Since the remarkable invention of the ruthenium-based DSC, with an efficiency of 7%, by O'Regan and Grätzel in 1991 [9], and subsequent improvements in DSC efficiency to 10% by the same group in 1993 [10], tremendous efforts have been expended by several groups concerning the development of DSC technology. The main factors that affect the efficiency and photovoltaic parameters of DSCs may be divided into the following categories: (i) dye structure; (ii) TiO_2 thin film (thickness, crystallinity and morphology); (iii) electrolyte composition; (iv) cell fabrication techniques. A major objective of this article is to familiarize coordination chemists (and others) with recent developments in strategies for the structural design of ruthenium photosensitizers to achieve an efficient photon-to-current conversion efficiency (η). This review is organized based on molecular engineering of ruthenium photosensitizers with: (1) 2,2′-bipyridine-based ligands; (2) 1,10-phenanthroline-based and dipyridylamine-based ligands; (3) a modified anchoring ligand; (4) thiocyanate-free; (5) other classes. Such structural modifications that affect on the fundamental photophysical and electrochemical properties as well as photovoltaic and cell η on DSCs are scrutinized.

2. Principle of DSCs

A typical DSC consists of five components: (i) a photoanode, (ii) a mesoporous semiconductor (TiO_2), (iii) a sensitizer (dye), (iv) a redox electrolyte and (v) a counter electrode. The working principle [11,12] of DSCs is shown schematically in Fig. 1.

The light absorbing dye adsorbed onto TiO_2 absorbs photons and goes to the excited state, and injects electrons into the conduction band (CB) of TiO_2. This leads to charge separation at the interface. The oxidized dye is subsequently reduced by electron
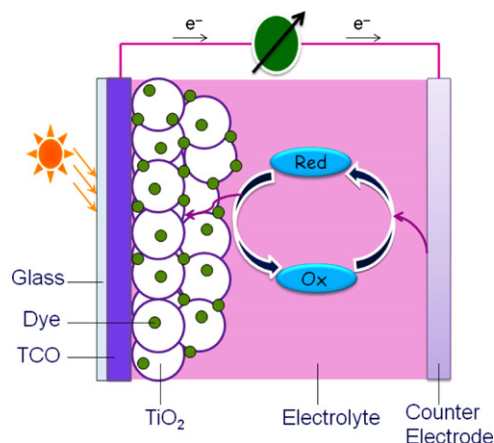

Fig. 1. Schematic illustration of the working principle of dye-sensitized solar cells. TCO = transparent conducting oxide; electrolyte = iodide/triiodide (I^-/I_3^-).

donation from an electrolyte containing an iodide/triiodide (I^-/I_3^-) redox system. The injected electrons diffuse through the semiconductor network to arrive at the back contact and then through the external load to the counter electrode. At the counter electrode, the reduction of I_3^- regenerates I^- through the donation of electrons from the external circuit, which completes the circuit.

The photosensitizer contains an anchoring ligand and an ancillary ligand. The anchoring ligand, in most cases, is H_2dcbpy and the carboxylic acid groups can be utilized for anchoring with TiO_2. In the design of a photosensitizer for DSC, most modifications involve the appropriate choice of an ancillary ligand for achieving better light harvesting. The proportional distribution of various photosensitizers is shown in Chart 1.

2.1. Basic features of an efficient Ru(II)-based sensitizer

- The wide absorption range and high molar absorption coefficient (ε) of the MLCT band(s).
- The highest-occupied molecular orbital (HOMO) localized on the mixed Ru(II)-t_{2g} and NCS-π orbital (or carbanionic part in case of —NCS free and C—H activated dyes), and the lowest-unoccupied molecular orbital (LUMO) located on the anchoring ligand.
- Energy level of the LUMO higher than CB of TiO_2 and the HOMO lower than I^-/I_3^- redox couple for efficient electron injection and dye regeneration, respectively.
- Long-term stability of the dye loaded onto the TiO_2 surface under thermal stress and light soaking.

3. Various classes of ruthenium DSCs with liquid electrolytes

3.1. Ruthenium photosensitizers with 2,2′-bipyridine-based ancillary ligands

Since the development of ruthenium sensitizers, **N3** [9,10], **N719** [10,13] and black dye [14], which show excellent DSC performance, many research groups have attempted to modify their structures with the goal of improving photovoltaic performance. The molecular structure of the **N3** dye consists of two anchoring ligands for connecting to the TiO_2 surface and two NCS for balancing the charge of the Ru metal (Fig. 2). In an effort to improve the light-harvesting ability of the photosensitizer, several modifications were made in the 2,2′-bipyridine (bpy) moiety, both in anchoring as well as ancillary ligands. The variation of substituents in the bpy ligand of Ru sensitizers and their corresponding DSC photovoltaic properties are listed in Table 1 and the effects of structural engineering on
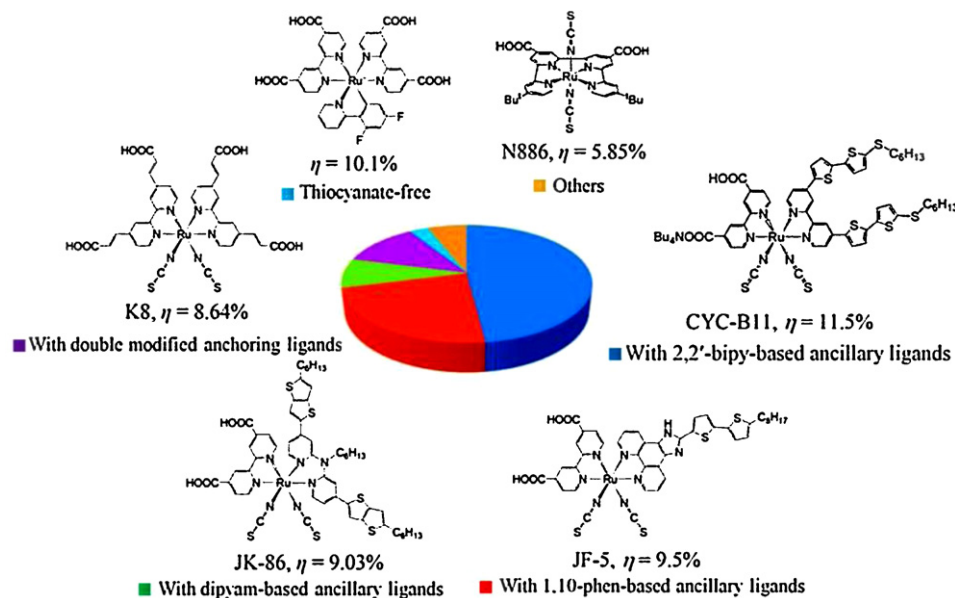
Chart 1. The proportional distribution of ruthenium photosensitizers with examples from each category and their photon-to-current conversion efficiency.

fundamental properties, such as absorption and redox behavior and photovoltaic parameters with respect to standard **N3** and/or **N719** dye are discussed.

The two acidic protons of the **N3** dye may dissociate at a pK_a of 1.5 and the resulting dianionic salt is referred to as the **N719** dye. Relative to the **N3** dye, the **N719** dye exhibits a high ε value and the Ru(III/II) redox potential is negatively shifted due to the replacement of H$^+$ with a tetraalkylammonium cation (Table 2), and also the doubly protonated form of **N3** is superior to the neutral **N3** dye for sensitization of nanocrystalline TiO$_2$ films [13].

A series of amphiphilic heteroleptic Ru-bpy sensitizer dyes substituted with alkyl chains of various lengths at the 4,4′-positions on one of the bpy ligands were developed (**1–5**). The lowest MLCT band of these complexes (**1–5**) was blue-shifted with lower ε values compared with the homoleptic **N3** dye (Table 2) [15,16]. For instance, dyes **2** (**N820**) and **4** (**Z907**) show a blue-shift of 360 and 280 cm^{-1}, respectively, relative to the **N3** dye along with a lower ε value. This is due to electron-donating nature of the alkyl groups at the 4,4′-positions of the bpy ligand resulting the π^* orbital of the ligands at a higher energy compared with that of dcbpy. Consequently, Ru(III/II) oxidation potential of **N3** complex is higher than the alkyl chain substituted complexes reflecting strong electron-withdrawing nature of the dcbpy ligand.

With the aim of protecting the dye layer against the ingression of water from the electrolyte and hence to enhance device stability, these hydrophobic dyes were examined under identical conditions of cell fabrication and measurement [17]. Such alkyl chains function as an electrical insulating barrier layer between the

sensitizer dye and the hole-transporting medium, thereby reducing interfacial charge recombination (CR) losses and increasing the open circuit potential (V_{OC}) and short-circuit photocurrent (J_{SC}). Hence, the V_{OC} of the DSCs is in the descending order of alkyl chain length C13 (**N621**) $\approx$ C9 (**Z907**) > C6 (**N820**) $\approx$ C1 (**KD1**) (**2–5**) [16], which is consistent with the efficiency trend with improved device stability under thermal stress and light soaking [18]. However, the C18 dye deviates from the series for the following reasons: (a) retardation of the regeneration reaction with increasing chain length and in particular, C18 dye shows 700-fold lower regeneration rate constant [16]; (b) slower charge recombination between the electrolyte and the injected electron [17]; and (c) faster recombination rate between the dye and the injected electron [18]. These drawbacks were reflected in the significantly reduced device performance of the C18 dye. Furthermore, the inhomogeneous dye-loading on the TiO$_2$ surface due to the folding of the long C18 chains along with incomplete swelling of the long C18 chains, thereby reduces the recombination blocking effect of the alkyl chain spacer [19].

A series of **N3**-related Ru(II)-sensitizers that contained 4,4′-di(p-X-phenyl)-2,2′-bipyridine (X = CN, F, H, OMe, NMe$_2$) as an ancillary ligand showed a systematic bathochromic shift in the MLCT band on traversing from electron-withdrawing to electron-donating congeners (**7–12**). In comparison with the **1** (**KD1**) dye, substitution with phenyl group allows **7** (**dye-1**) to exhibit a 350 cm^{-1} red-shifted MLCT absorption with higher ε value, resulting in higher cell η, under identical conditions [15]. For the complexes **9–11** and **N3**, the cell η increases with increasing electron-donating power: F (**9**) < COOH (**N3**) < H (**10**) < OMe (**11**). In contrast, strongest electron-donating (NMe$_2$-based) and strongest electron-withdrawing (CN-based) devices showed inferior device performance. The CR kinetics between the injected electrons and the oxidized dye is in the order CN (**8**) > COOH (**N3**) > F (**9**) > H (**10**) > OMe (**11**). This fast CR in CN-based device is caused by the electronic characteristics, resulting in poor device performance and for the NMe$_2$-based dye, is probably due to fast CR dynamics between the injected electrons and the oxidized electrolyte and also the ruthenium sensitizer in the excited state (Dye$^{\bullet+}$) is quenched by I$^-$ [20]. It has been shown that amines interact with I$_2$ to form charge transfer complex and this might lead to an increase in the amount of oxidized electrolyte that comes into contact with the dyes, thereby enhancing CR.
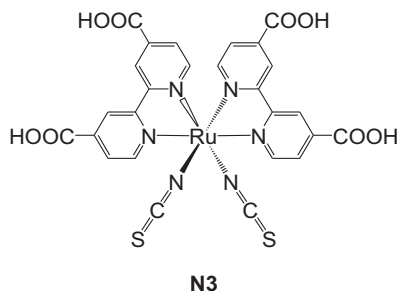

Fig. 2. Molecular structure of the **N3** dye.

Table 1
Molecular structures of ruthenium photosensitizers with various bipyridine-based ancillary ligands and photovoltaic properties of corresponding DSCs.

General formula:
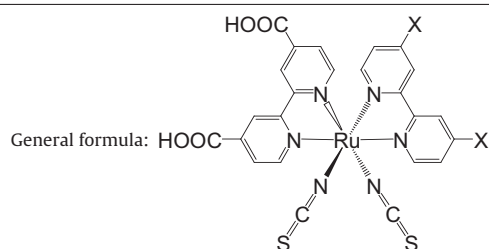
No	X (code)	J_{SC}, (mA cm^{-2})	V_{OC} (V)	FF	η (%)	Ref.
N3	•—COOH	18.2	0.72	0.73	10.0[a]	[10]
1	H (**KD1**)	10.4	0.53	0.62	4.5[b]	[15]
2	•—CH$_3$ (**N820**)	14.7	0.70	–	6.7[c]	[16]
3	•—C$_6$H$_{13}$	15.5	0.70	–	7.4[c]	[16]
4	•—C$_9$H$_{19}$ (**Z907**)	16.0	0.74	0.67	8.4[c]	[16]
5	•—C$_{13}$H$_{27}$ (**N621**)	16.2	0.74	0.72	8.6[c]	[16]
6	•—C$_{18}$H$_{37}$	3.5	0.67	0.56	1.3[d]	[17]
7	(**dye-1**)	12.6	0.57	0.58	5.5[b]	[15]
8	—CN	10.0	0.67	0.74	4.9[e]	[20]
9	—F	14.3	0.72	0.73	7.6[e]	[20]
10	—H	15.2	0.71	0.72	7.8[e]	[20]
11	—OMe	16.0	0.72	0.72	8.3[e]	[20]
12	—NMe$_2$	8.4	0.69	0.73	4.2[e]	[20]
13	(**Z910**)	17.2	0.78	0.76	10.2[f]	[22]
14	—C$_6$H$_{13}$ (**K-19**)	14.6	0.71	0.67	7.0[f,g]	[23]
15	(**K77**)	19.2	0.78	0.72	10.5[f]	[24]

Table 1 (*Continued*)
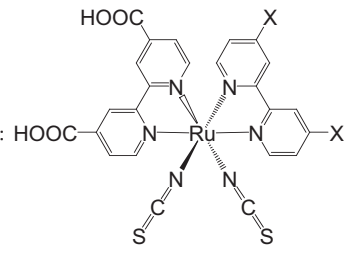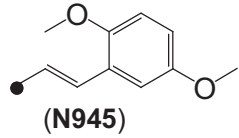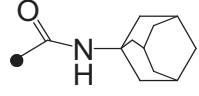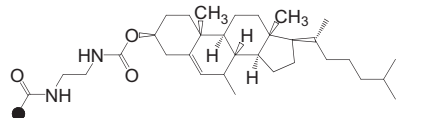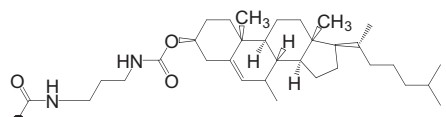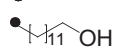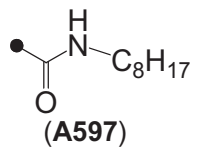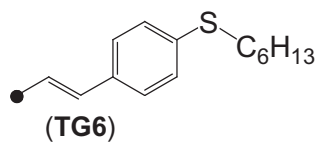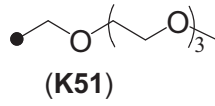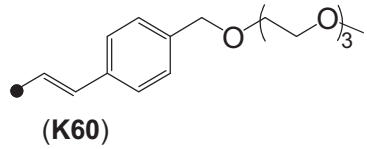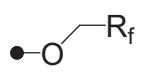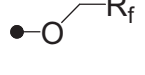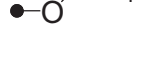
General formula:

No	X (code)	J_{SC}, (mA cm^{-2})	V_{OC} (V)	FF	η (%)	Ref.
16	(**N945**)	16.5	0.79	0.72	9.6[f]	[26]
17		15.8	0.69	0.66	7.0[f]	[27]
18		15.5	0.68	0.71	7.4[f]	[27]
19		16.1	0.68	0.7	7.6[f]	[27]
20		17.5	0.70	0.72	8.8[f]	[27]
21	(**A597**)	11.8	0.78	0.78	7.3[h]	[28]
22	(**TG6**)	14.0	0.75	0.55	5.8[i]	[29]
23	(**K51**)	15.4	0.74	0.69	7.8[j]	[30]
24	(**K60**)	16.9	0.73	0.69	8.4[f]	[33]
25	$R_f = C_2F_4H$ (**CT4**)	13.3	0.67	0.70	6.2[k]	[34]
26	$R_f = C_3F_7$ (**CT7**)	15.4	0.68	0.66	6.9[k]	[34]
27	$R_f = C_4F_8H$ (**CT8**)	15.0	0.68	0.67	6.8[k]	[34]

Table 1 (*Continued*)
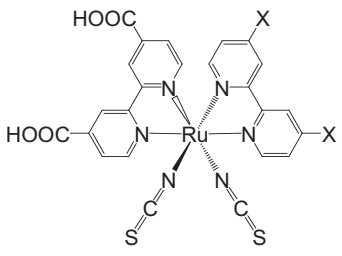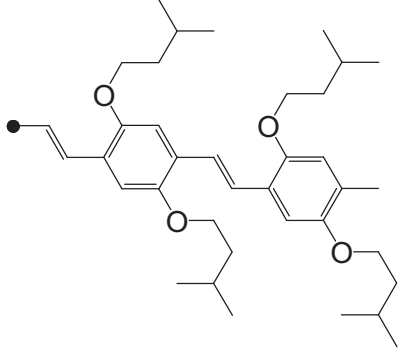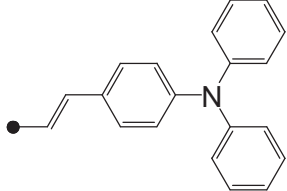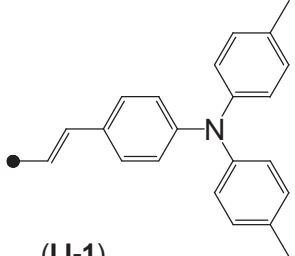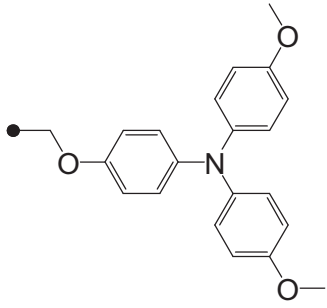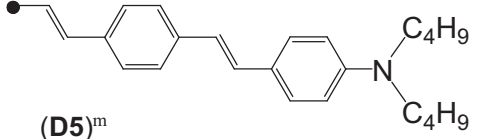
General formula:

No	X (code)	J_{SC}, (mA cm^{-2})	V_{OC} (V)	FF	η (%)	Ref.
28	(**DCSC13**)	10.1	0.73	0.69	5.1[l]	[35]
29	(**Ru-bpy–TPA**)	–	–	–	–	[36]
30	(**IJ-1**)	17.6	0.80	0.73	10.3	[37]
31	(**N845**)[m]	–	–	–	–	[38]
32	(**D5**)[m]	10.8	0.63	0.68	4.6[c,n]	[40]

Table 1 (*Continued*)
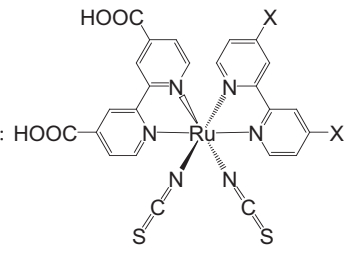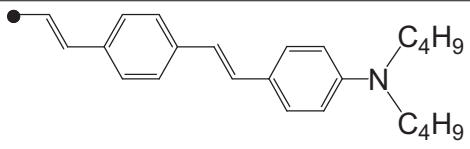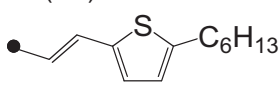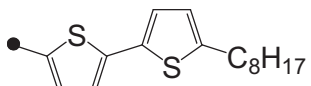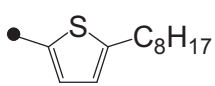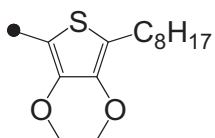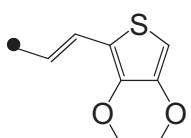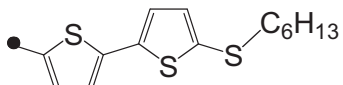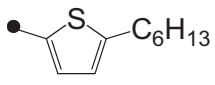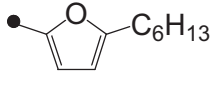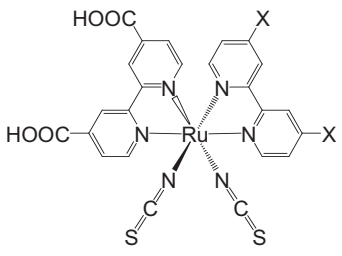
General formula:

No	X (code)	J_{SC}, (mA cm^{-2})	V_{OC} (V)	FF	η (%)	Ref.
33	(**D6**)	11.7	0.63	0.66	4.8[c,n]	[40]
34	(**HRS-1**)	20.0	0.68	0.69	9.5[o]	[41]
35	(**CYC-B1**)	23.9	0.65	0.55	8.5[p]	[42]
36	(**CYC-B3**)	15.7	0.67	0.71	7.4[q]	[43]
37	(**SJW-E1**)	21.6	0.67	0.63	9.0[q]	[43]
38	(**Ru-EDOT**)	19.1	0.66	0.72	9.1	[44]
39	(**CYC-B11**)	20.1	0.74	0.77	11.5	[46]
40	(**C101**)	18.6	0.74	0.75	10.5	[47]
41	(**C102**)	17.8	–	–	9.5	[47]

Table 1 (*Continued*)

General formula:
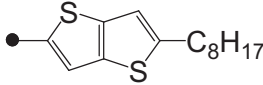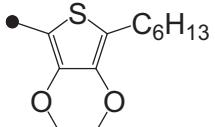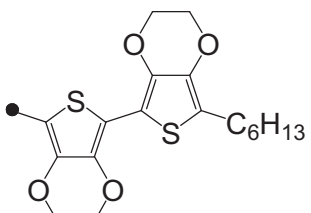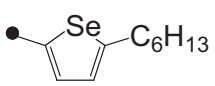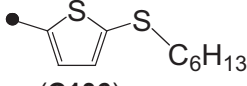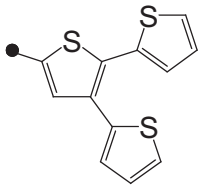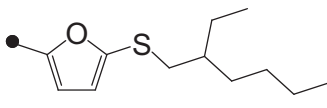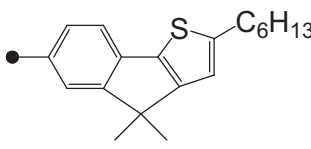
No	X (code)	J_{SC}, (mA cm^{-2})	V_{OC} (V)	FF	η (%)	Ref.
42	(C104)	17.9	0.76	0.78	10.5	[48]
43	(C103)	18.3	0.76	0.75	10.4	[49]
44	(C107)	19.2	0.74	0.75	10.7	[49]
45	(C105)	18.7	0.75	0.75	10.6	[50]
46	(C106)	19.2	0.78	0.76	11.3	[51]
47	(3T)	15.5	0.68	0.70	7.4	[52]
48	(LXJ-1)	16.5	0.72	0.75	8.8[r]	[53]
49	(JK-188)	18.6	0.72	0.71	9.5[s]	[54]

Table 1 (*Continued*)
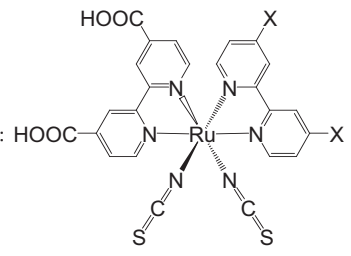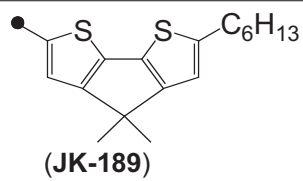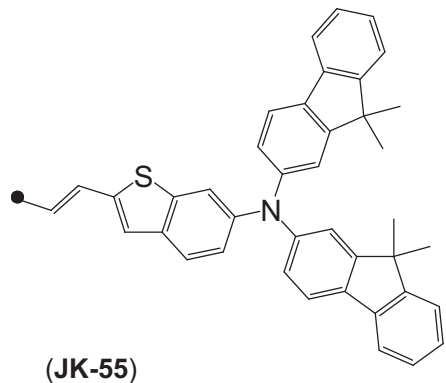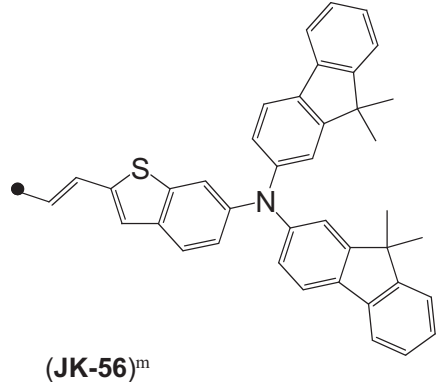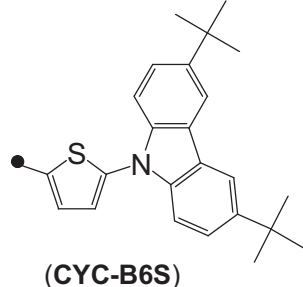
General formula:

No	X (code)	J_{SC}, (mA cm^{-2})	V_{OC} (V)	FF	η (%)	Ref.
50	(**JK-189**)	18.9	0.63	0.73	8.7[s]	[54]
51	(**JK-55**)	17.6	0.64	0.72	8.2[t]	[55]
52	(**JK-56**)[m]	17.5	0.71	0.73	9.2[t]	[55]
53	(**CYC-B6S**)	19.8	0.78	0.63	9.7[u]	[56]

Table 1 (Continued)

General formula:

No	X (code)	J_{SC}, (mA cm^{-2})	V_{OC} (V)	FF	η (%)	Ref.
54	(CYC-B6L)	18.2	0.78	0.63	9.0[u]	[56]
55	(CYC-B13)	10.3	0.73	0.68	5.1[v]	[57]
56	(CYC-B7)	17.4	0.79	0.65	9.0	[58]

● Indicates the point of attachment of the substituent to the ancillary ligand.

[a] Conditions: 96.0 mW/cm^2 simulated AM 1.5 solar radiation; in a mixture of (90:10, v/v) acetonitrile and 3-methyl-2-oxazolidinone, 0.3 M LiI and 0.03 M I$_2$.

[b] Conditions: 75.0 mW/cm^2 simulated AM 1.5 solar radiation; in a mixture of (1:1, v/v) acetonitrile and propylene carbonate, 0.5 M LiI and 0.05 M I$_2$; cell area: 0.15 cm^2.

[c] Standard global AM 1.5 solar radiation; in a mixture of (1:1, v/v) acetonitrile and valeronitrile, 0.6 M *N*-methyl-*N*-butylimidazolium iodide, 0.05 M LiI, 0.05 M I$_2$, 0.5 M *tert*-butylpyridine.

[d] Under identical condition **N621** shows η = 3.2%.

[e] Conditions: 100 mW/cm^2 simulated AM 1.5 solar radiation, under identical condition **N3** shows η = 7.8%.

[f] Standard global AM 1.5 solar radiation; in a mixture of (3:1, v/v) acetonitrile and valeronitrile, 0.6 M 1-propyl-3-methylimidazolium iodide (PMII), 0.13 M GuNCS, 0.03 M I$_2$, 0.5 M *tert*-butylpyridine.

[g] Under identical condition **Z907** and **N719** show η = 6.0 and 6.7%, respectively.

[h] Under identical condition **Z907** shows η = 8.3%.

[i] Under identical condition **N719** shows η = 5.5%.

[j] Under identical condition **Z907** shows η = 6.6%.

[k] Under identical condition **N719** shows η = 7.3%.

[l] Under identical condition **N820** shows η = 4.4%.

[m]The structure contains only one substituent for X, another X is CH$_3$.

[n] Under identical condition **N3** shows η = 4.1%.

[o] Under identical condition **N719** shows η = 8.9%.

[p] Under identical condition **N3** shows η = 7.7%.

[q] Under identical condition **N3** shows η = 8.4%.

[r] Under identical condition **Z907** shows η = 8.4%.

[s] Under identical condition **Z907** shows η = 9.0%.

[t] Under identical condition **Z907** shows η = 8.8%.

[u] Under identical condition **N3** shows η = 8.5%.

[v] Under identical condition **CYC-B6S** shows J_{SC} = 9.2, V_{OC} = 0.73, FF = 0.70, η = 4.7%.

Table 2
Absorption and electrochemical data for standard dyes and entries **1–5**.

No	Code	λ_{max} (nm) (ε (10^4 M^{-1} cm^{-1}))[a]			E_{ox} of Ru(III/II) (V vs. SCE)[b]	Ref.
		π–π^*	π–π^* or dπ–π^*	dπ–π^*		
	N3	314 (4.82)		398 (1.40) 534 (1.42)	0.85	[10]
	N719	312 (4.91)		395 (1.43) 535 (1.47)	–	[13]
1	KD1			527 (0.78)[b]	0.73	[15]
2	N820	295 (4.54)	312 (3.35)	383 (1.13) 524 (1.16)	0.78	[16]
3		296 (4.26)	312 (3.20)	384 (1.01) 525 (1.11)	0.73	[16]
4	Z907	295 (4.24)	312 (3.01)	385 (1.09) 526 (1.16)	0.74	[16]
5	N621	296 (4.21)	312 (3.02)	384 (1.08) 525 (1.15)	0.74	[16]

[a] In EtOH.
[b] In DMF.

Table 3
Absorption and electrochemical data for standard dye and entries **13–16**.

No	Code	λ_{max} (nm) (ε (10^4 M^{-1} cm^{-1}))[a]			E_{ox} of Ru(III/II) (V vs. SCE)	Ref.
		π–π^*	π–π^* or dπ–π^*	dπ–π^*		
4	Z907	295 (4.24)	312 (3.01)	385 (1.09) 526 (1.16)	0.74	[16]
13	Z910			410 (1.70) 543 (1.69)	0.73[a]	[22]
14	K-19		320 (5.12)	360 (4.76) 543 (1.82)[b]	0.71[c]	[23]
15	K77		310 (5.12)	346 (4.76) 546 (1.94)[c]	0.73[c]	[24]
16	N945H	305 (5.63)	316 (6.07)	394 (3.45) 550 (1.89)[b]	0.57[c]	[26]

[a] In MeCN.
[b] 1:1 MeCN-^{t}BuOH.
[c] DMF.

Light absorption can be enhanced in heteroleptic Ru(II) complexes by endowing them with electron-donating alkoxy groups, which accomplish new amphiphilic sensitizers (**13–16**) with broad coverage of the visible spectrum (Table 3). The ε and cell η follow the order: **Z910 > Z907 > N719** [21,22].

Further improvements have been made, with cell η > 10%, by the substitution of a —OMe group of the **Z910** dye with more hydrophobic analogs viz. —OC$_6$H$_{13}$ **14** (**K-19**) and —O^{t}Bu **15** (**K-77**) group at styryl moieties of the amphiphilic heteroleptic Ru-complexes [23–25]. The ε value for MLCT absorption of the **14** (**K-19**) dye is higher than that of the standard **Z907**, **N719** and **Z910** dyes (Table 3). This fostered applications and devices based on **14** (**K-19**) exhibited better cell η compared with the **Z907** and **N719**, along with better stability under thermal stress and light soaking, due to the stronger adsorption of the **14** (**K-19**) dye by the presence of the long alkyl chains [23]. A most striking breakthrough, however, was achieved in the case of the **15** (**K-77**) dye. Light harvesting by the lowest energy MLCT band was improved further compared with **14** (**K-19**) dye and the cell η reached 10.5% [24].

Excited-state directionality i.e. efficient electron transfer from the Dye$^{\bullet+}$ to the TiO$_2$ conduction band is another essential requirement for DSCs. For example, the monoanionic Bu$_4$N[Ru(Hdcbpy)(L^1)(NCS)$_2$] **16** (**N945H**) dye showed a 830 cm^{-1} red-shifted absorption compared with **Z910** and the ε value follows the order: **N945H > Z910 > N3** (Table 3) [26]. The photovoltaic data for the dianionic **16** (**N945**) dye showed a superior cell η compared with the standard dianionic dye **N719**. In comparison with the **14** (**K-19**) dye, **16** (**N945**) exhibits a higher cell η value. This is probably due to the incorporation of donor groups in the *ortho* and *meta* positions of the extended π conjugated system that increased the LUMO energy level without disturbing the HOMO level and thereby increasing the driving force for electron injection into TiO$_2$ by adjusting the electron densities of the donor moieties.

In a search for more amphiphilic heteroleptic Ru(II) dyes, amide-functionalized ligands L^2, L^3, L^4 and alkylhydroxy ligand L^5 and corresponding sensitizers (**17–20**) were synthesized [27]. However, all of the dyes show a lower ε value for MLCT absorption (Table 4) along with a low cell η compared with homoleptic **N3** dye and among these dyes, dye **20** yielded a better cell η value of 8.8%.

Hallett and Jones [28] synthesized **21** (**A597**), a ruthenium sensitizer, comprised of a doabpy as an ancillary ligand. Although **21** (**A597**) exhibited favorable absorption and redox behavior in solution (Table 4), the cell η was lower than **Z907**, under identical conditions. The reason for the lower cell η could be due to the poor light harvesting of the dye after anchored onto TiO$_2$ films and/or a faster CR phenomenon.

The publication by O'Regan, Ghaddar and co-workers [29] describes the **22** (**TG6**) dye, with a —SC$_6$H$_{13}$ group as the electron donor along with styryl π conjugation at the 4,4′-positions of the bpy ligand. This monoanionic dye showed better visible light harvesting compared with the —OC$_6$H$_{13}$ substituted **14** (**K-19**) dye. The presence of a sulfur atom in the aliphatic chain may be appreciated by comparing the HOMO–LUMO energy gap of **22** (**TG6**) (2.50 eV) with that of the **N3** (2.60 eV) determined by density functional theoretical calculations and a fast electron injection dynamics into TiO$_2$ CB is seen, as the excited-state oxidation potential (E^*_{ox}) of the **22** (**TG6**) was −0.13 V more negative compared with that of the **N719**. Furthermore, interfacial recombination between an injected electron and the electrolyte was increased using **22** (**TG6**) dye, may be due to the extended π-conjugation and this could be valid for any dye with an extended π-conjugation.

A unique class of solar cells comprised of ion-coordinating sensitizers, induce a striking improvement in η compared with a non ion-coordination analog [30–32]. For instance, the **23** (**K51**) dye is an analog of **Z907**, in which hydrophobic alkyl chains have been replaced with ion-coordinating oxyethylene side chains. Both dyes showed similar light absorption behavior. However, the cell η value of **23** (**K51**) is 7.8%, which is higher than that of **Z907**, due to faster rate of dye regeneration for the former [30]. When lithium ions with concentration equal to the dye adsorbed on the surface of the TiO$_2$ surface were added to the liquid electrolyte, the **Z907** dye exhibited a decrease in V_{OC} and an increased J_{SC} and a counter balance of the parameters resulted in the same efficiency. In contrast, in such a situation, the **23** (**K51**) dye shows Li$^+$ "ion-trapping" functionality and inhibits the adsorption of Li$^+$ on the TiO$_2$ surface and shows

Table 4
Absorption and electrochemical data for entries **17**–**21**.

No	Code	λ_{max} (nm) (ε (10^4 M^{-1} cm^{-1}))[a]			E_{ox} of Ru(III/II) (V vs. SCE)[a]	Ref.
		$\pi-\pi^*$	$\pi-\pi^*$ or $d\pi-\pi^*$	$d\pi-\pi^*$		
17			313 (3.88)	392 (1.17) 537 (1.19)	0.84	[27]
18			314 (3.36)	390 (1.11) 531 (1.12)	0.84	[27]
19			312 (3.39)	393 (1.12) 533 (1.21)	0.85	[27]
20		297 (4.54)	309 (2.74)	370 (1.25) 522 (1.26)	0.75	[27]
21	(**A597**)	297 (4.54)	313 (5.23)	397 (1.60) 539 (1.75)	0.92	[28]

[a] In DMF.

Table 5
Absorption and electrochemical data for entries **29**–**31**.

No	Code	λ_{max} (nm) (ε (10^4 cm^{-1}))[a]			E_{ox} of Ru(III/II) (V vs. SCE)[a]	Ref.
		$\pi-\pi^*$	$\pi-\pi^*$ or $d\pi-\pi^*$	$d\pi-\pi^*$		
29				430 (5.71) 540 (2.00)	–	[36]
30	**IJ-1**			432 (4.34) 536 (1.91)	0.94	[37]
31	**N845**	300 (5.52)	312 (4.41)	372 (1.05) 535 (1.10)	0.98	[38]

[a] In DMF.

potential invariance on the TiO$_2$ conduction band, with a striking improvement in J_{SC} and V_{OC} values. At higher Li$^+$ concentration, the excess Li$^+$ is adsorbed on the TiO$_2$ surface resulting in a slight drop in V_{OC} value, but the J_{SC} value is increased as the TiO$_2$ surface adapts to a globally positive charge and hence a greater local concentration of I$^-$ and increased dye regeneration rate [31].

However, the **23** (**K51**) dye had poor stability towards continuous thermal stress at 80 °C due to desorption into the electrolyte, because of the presence of oxyethylene chains, which conferred an increase in solubility. In order to reduce its solubility, the dye [Ru(H$_2$dcbpy)(L^6)(NCS)$_2$] **24** (**K60**), which has a ligand with more extended π-conjugation and ion-coordinating oxymethylene chains, was developed [33]. The effect of Li$^+$ ion on the photovoltaic parameters of the dye **24** (**K60**) is similar to that of the dye **23** (**K51**). The device containing the **24** (**K60**) dye exhibited good stability and maintained more than 93% of the initial photovoltaic performance upon aging at 80 °C under dark conditions or at 60 °C under visible light soaking (100 mW/cm^2).

Lin and co-workers [34] reported on the synthesis of a series of fluorous amphiphilic ruthenium sensitizers **25** (**CT4**), **26** (**CT7**) and **27** (**CT8**). The **26** (**CT7**) and **27** (**CT8**) dyes exhibit cell η values that are comparable with that of standard **N719**, and outperformed the **Z907** dye. The main reason for these superior efficiencies is due to the presence of hydrophobic fluorous chains, which allow these dyes to adsorb on the TiO$_2$ surface more strongly and provide higher dye density than alkyl chains in the case of the **Z907** dye.

The [Ru(H$_2$dcbpy)(L^7)(NCS)$_2$] **28** (**DCSC13**) dye illustrates the incorporation of L^7 donor group enhances ε of MLCT absorption band relative to that of **2** (**N820**) dye. It also inhibits the I$_3^-$ in the electrolyte from recombining with e$^-$(TiO$_2$), resulting in reduced interfacial recombination and hence, increased V_{OC} value compared with that of the **N820** dye. The drawback of the **28** (**DCSC13**) dye is the fact that bulky groups make the dye size bigger and reduce the density of the dye on the TiO$_2$ surface. Nevertheless, under identical conditions, both the V_{OC} and cell η of the **28** (**DCSC13**) sensitizer are higher than **2** (**N820**), besides 40% less adsorption of molecules onto the TiO$_2$ for the former [35].

A new series of "donor–acceptor" dyes involving π-conjugation with a covalently attached pendant triphenylamine (TPA) hole accepting moiety have been extensively studied in DSCs [36–39]. A comparison between dyes **29** (Ru-bpy–TPA) and **2** (**N820**) indicates that, although the values for ε and cell η have been greatly enhanced for the former (Table 5), the CR kinetics are not influenced by the TPA units [36]. Similar to **29** (Ru-bpy–TPA), a methyl substituted

TPA-donor antenna dye **30** (**IJ-1**) also showed enhanced ε and cell η values compared with **2** (**N820**) [37].

However, when an arylamine-based secondary electron donor group (L^8) is employed in the dye, [Ru(H$_2$dcbpy)(L^8)(NCS)$_2$] **31** (**N845**), an interface between the hole and the TiO$_2$ nanostructures is developed [38]. The **31** (**N845**) dye displayed recombination dynamics three orders of magnitude less than the **N719** dye. In addition, the long distance between the hole and TiO$_2$ results a long-lived charge-separated pair, which is highly desirable for efficient DSCs. Incidentally, —SCN free aryl-TPA-based **N3**-analogs have also shown similar long-lived charge-separation states [39].

Extended π-conjugation of oligophenylenevinylene groups at the 4,4′-position of the bpy in **32** (**D5**) and **33** (**D6**), allows these two dyes to exhibit better light absorption compared with **N3** dye (Table 6) and the J_{SC} and cell η values follow the order: **D6** > **D5** > **N3**. In contrast, V_{OC} of the **32** (**D5**) and **33** (**D6**) dyes remain same compared with **N3** dye. This is probably due to the fact that sensitizers **32** (**D5**) and **33** (**D6**) are unable to form hydrophobic layers around TiO$_2$ and thus are not able to minimize the back electron transfer from e$^-$(TiO$_2$) to I$_3^-$. Nevertheless, **32** (**D5**) and **33** (**D6**) dyes adhere more strongly on the TiO$_2$ surface than the **N3** dye, hence showing long-term stability [40].

Yanagida and co-workers [41] employed a Ru sensitizer **34** (**HRS-1**), consisting of a hybrid of long alkyl chain containing thienyl-vinyl-conjugated bpy ligand as an ancillary ligand. The hydrophobic characteristics of the long hexyl chains aid in (i) reducing the interfacial recombination of e$^-$(TiO$_2$) → I$_3^-$; (ii) preventing water from reaching the surface of the TiO$_2$ and dye leaching, which thereby increases the stability of the devices. Furthermore, **34** (**HRS-1**) dye exhibits an enhanced cell η than that of **N719**.

The potential of thiophene-based ancillary ligands on Ru-based DSCs was developed by Wu and co-workers [42]. A bis-thiophene substituted efficient electron donor group containing the Ru sensitizer, **35** (**CYC-B1**), showed a dramatic effect on photophysical properties (Table 7) and device performance. A 100 mV cathodic shift of $E_{1/2}^{Ru(III/II)}$ in **35** (**CYC-B1**) reflects the more electron-donating property of the alkylbis-thiophene-bpy compared with that for the dcbpy ligand in **N3**. Such rich fundamental properties make the performance of the **35** (**CYC-B1**) dye more efficient in the DSC than **N3**, under identical conditions.

The dye **36** (**CYC-B3**) [43], which contains one less thiophene unit than **35** (**CYC-B1**), causes diminished light absorption (Table 7) along with a lower solubility, making this dye inferior toward photovoltaic cells, in comparison with that of the **35** (**CYC-B1**). The

Table 6
Absorption data for entries **32–33**.

No	Code	λ_{max} (nm) (ε (10^4 M^{-1} cm^{-1}))[a]		Ref.
		$\pi-\pi^*$ or $d\pi-\pi^*$	$d\pi-\pi^*$	
32	D5	441 (4.03)	527 (2.60)	[40]
33	D6	449 (7.85)	539 (3.43)	[40]

[a] In DMF.

Table 7
Absorption and electrochemical data for standard dye and entries **34–37**.

No	Code	λ_{max} (nm) (ε (10^4 M^{-1} cm^{-1}))			E_{ox} of Ru(III/II) (V vs. SCE)	Ref.
		$\pi-\pi^*$	$\pi-\pi^*$ or $d\pi-\pi^*$	$d\pi-\pi^*$		
34	HRS-1		371 (4.24)	542 (1.87)[a]	0.80[a]	[41]
35	CYC-B1	312 (3.58)	400 (4.64)	553 (2.12)[b]	0.76[b]	[42]
36	CYC-B3	320 (5.23)	370 (3.30)	544 (1.57)[b]	–	[43]
37	SJW-E1			546 (1.87)[b]	–	[43]

[a] In EtOH.
[b] DMF.

Table 8
Absorption and electrochemical data for entries **38–39**.

No	Code	λ_{max} (nm) (ε (10^4 M^{-1} cm^{-1}))[a]			E_{ox} of Ru(III/II) (V vs. SCE)[a]	Ref.
		$\pi-\pi^*$	$\pi-\pi^*$ or $d\pi-\pi^*$	$d\pi-\pi^*$		
38	Ru-EDOT			538 (1.60)	0.65	[44]
39	CYC-B11	320 (4.55)	380 (5.40)	554 (2.42)	0.72	[46]

[a] In DMF.

introduction of electron-donating EDOT instead of a thiophene moiety in **37** (**SJW-E1**) dye resulted in an enhanced ε of MLCT band compared with **36** (**CYC-B3**) [43].

In summary, the relative cell η follows the order: **35** (**CYC-B1**) > **37** (**SJW-E1**) $\approx$ **34** (**HRS-1**) > N3 > **36** (**CYC-B3**) dyes. Of note, the MLCT ε value of the N3 dye is lower than that of **36** (**CYC-B3**), but the cell η is still higher. Electrochemical impedance spectroscopy (EIS) data in the form of a Bode phase plot show that the lifetime of the e$^-$(TiO$_2$) is, in descending order: N3 > **37** (**SJW-E1**) > **36** (**CYC-B3**). This probably accounts for the higher η of N3 although it shows moderate light-harvesting ability.

In the case of the **38** (**Ru-EDOT**) dye [44], the following changes have been made: an increase in the electron-donating ability of the thiophene moiety by the EDOT group along with extending π conjugation and the simultaneous removal of the long alkyl chain. The higher ε of MLCT band and cathodically shifted $E_{1/2}^{Ru(III/II)}$ values for **38** (**Ru-EDOT**) relative to those of N3 dye reflects the influence of the new, electron-rich ligand (Table 8). This dye exhibits a similar ion-coordinating effect when Li$^+$ ions are added [45].

Replacement of the hexyl-terminal chain in **35** (**CYC-B1**) with an electron-rich hexylthio-terminal chain in **39** (**CYC-B11**), causes the highest ε value (2.42×10^4 M^{-1} cm^{-1}) of the Ru(II)-sensitizers containing thiophene moieties discussed so far. A 40 mV cathodic shift in $E_{1/2}^{Ru(III/II)}$ of **39** (**CYC-B11**) relative to that of **35** (**CYC-B1**), reflects the influence of the sulfur atoms on electron donation and π-conjugation to the bpy ancillary ligand and on the metal complex

(Table 8) [46]. A device fabricated using the sensitizer **39** (**CYC-B11**), in the presence of a volatile liquid electrolyte showed an excellent cell η value of 11.5%.

The dye **40** (**C101**), contained a pendant hexyl chain in a thiophene, which was attached to a bpy unit shows long-term stability [47]. The MLCT absorption band of **40** (**C101**) is 803 cm^{-1} redshifted relative to **Z907** with enhanced ε value (Table 9) and it has a remarkable cell η of 11%.

Upon substitution of the thiophene group in **40** (**C101**) with the furan in **41** (**C102**), the cell η value was diminished [47]. This is probably due to the lower adsorbed dye density of the latter compared with the former on a TiO$_2$ surface. Hence, **41** (**C102**) dye coated cells are more exposed to the electrolyte and thus the CR rate is enhanced, resulting in a lower cell η value. The sensitizer **42** (**C104**) [48], which contained a thieno[3,2-b]thiophene moiety, exhibited a much higher ε at the MLCT band compared with that of **Z907** and thus, the cell η value is higher than that of the latter complex, under identical conditions.

Wang and co-workers [49] developed the ruthenium sensitizers, **43** (**C103**) and **44** (**C107**), containing EDOT and O-EDOT units, respectively, conjugated at the 4,4′-positions of a bpy ligand. The ε and cell η values follow the trend: **44** (**C107**) > **43** (**C103**) > **Z907** (Table 10). However, V_{OC} follows the reverse order as because lower dye density of the large ancillary ligand containing **44** (**C107**) dye, hence, CR is faster and thus V_{OC} value is lower than **43** (**C103**). The dye **45** (**C105**) [50] contains a selenophene unit conjugated with a bpy ligand coordinated with Ru(II). The ε value increases in

Table 9
Absorption data for entries **40–42**.

No	Code	λ_{max} (nm) (ε (10^4 M^{-1} cm^{-1}))[a]		Ref.
		$\pi-\pi^*$ or $d\pi-\pi^*$	$d\pi-\pi^*$	
40	C101		407 (1.80) 547 (1.75)	[47]
41	C102		407 (1.76) 547 (1.68)	[47]
42	C104	312 (5.50)	368 (4.75) 553 (2.05)	[48]

[a] In DMF.

Table 10
Absorption data for entries **43**–**46**.

No	Code	λ_{max} (nm) (ε ($10^4 M^{-1} cm^{-1}$))[a]		Ref.
		π–π^* or dπ–π^*	dπ–π^*	
43	C103		370 (3.55) 550 (2.05)	[49]
44	C107		453 (5.43) 559 (2.74)	[49]
45	C105	309 (3.95)	353 (3.35) 550 (1.84)	[50]
46	C106	310 (4.10)	348 (3.25) 550 (1.87)	[51]

[a] In DMF.

Table 11
Absorption data for entries **47**–**50**.

No	Code	λ_{max} (nm) (ε ($10^4 M^{-1} cm^{-1}$))		Ref.
		π–π^* or dπ–π^*	dπ–π^*	
47	3T	303 (5.06)	380 (2.84) 551 (1.70)[a]	[52]
48	LXJ-1	309 (4.65)	353 (3.24) 549 (1.84)[a]	[53]
49	JK-188		378 (4.26) 522 (1.56)[b]	[54]
50	JK-189		380 (3.07) 543 (1.59)[b]	[54]

[a] In DMF.
[b] EtOH.

the order of **45** (**C105**) > **40** (**C101**) > **41** (**C102**), consistent with the electropositivity and the size of the heteroatoms (Se > S > O) and photovoltaic parameters of **41** (**C102**) are parallel to that of the **40** (**C101**). The same effect on photophysical and photovoltaic parameters has been observed by replacing the hexyl-terminal chain in **40** (**C101**) with an electron-rich hexylthio-terminal chain in **46** (**C106**), as observed for **35** (**CYC-B1**) and **39** (**CYC-B11**). The ε value of MLCT band for **46** (**C106**) is higher than that of the **Z907** and **40** (**C101**) dyes (Table 10), and encouragingly, it has a cell $\eta = 11.3\%$ [51].

A dendritic terthiophene functionalized ruthenium sensitizer, **47** (**3T**), was developed by Grätzel, Bäuerle, and co-workers [52]. Although **47** (**3T**) showed better absorption behavior than **Z907** (Table 11), the non-planar configuration and β-substituent pattern on terthiophene restrict further enhancement in ε than **40** (**C101**). The sensitizer **48** (**LXJ-1**) containing an electron-rich thioalkoxyfuran unit at the 4,4′-positions of the bpy ligand, that is coordinated to ruthenium was developed by Li and co-workers [53]. The **48** (**LXJ-1**) dye shows 980 cm^{-1} red-shifted MLCT band compared with that of **Z907** (Table 11) and cell η value is enhanced relative to **Z907**, under identical conditions.

Ko and co-workers developed ruthenium sensitizers containing unsymmetrical indeno[1,2-b]thiophene **49** (**JK-188**) and a fused dithiophene unit **50** (**JK-189**) at the 4,4′-positions of the bpy [54]. The $E_{1/2}^{Ru(III/II)}$ of **50** (**JK-189**) is 60 mV cathodically shifted from that of the **49** (**JK-188**), attributed to the presence of better electron-donating dithiophene ring in the former dye. Under identical conditions, the device η follows the order: **49** (**JK-188**) > **N719** > **50** (**JK-189**). The superior cell η for **49** (**JK-188**) relative to **N719** is due to better light absorption. Of note, J_{SC} for the **50** (**JK-189**)-based cell is distinctly higher compared with **49** (**JK-188**) and **N719**; however, the V_{OC} value follows a reverse order by 90–130 mV, because of the decreased amount of dye-loading on TiO$_2$ (due to the size and structure of the dye), relative to **JK-188**, and hence, an increased rate of CR occurred.

The performance of a sensitizer does not depend entirely on ε values and energy level of the frontier orbitals. The structure and size of the dye also play pivotal roles. For example, with an antenna ligand, L^9, in Ru dyes, **51** (**JK-55**) and **52** (**JK-56**) (methyl and L^9 at 4 and 4′-positions, respectively, of bpy) a huge enhancement in ε of the MLCT band was observed (Table 12). Due to presence of a bulky structure, there is less dye coverage of the **51** (**JK-55**) giving rise to a large unoccupied area on the TiO$_2$ surface and hence, a higher dark current is seen and also the electron lifetime is inferior compared with the **52** (**JK-56**) dye. In the present case η follows the following trend: **52** (**JK-56**) > **N719** > **51** (**JK-55**) [55].

Two Ru sensitizers, **53** (**CYC-B6S**) and **54** (**CYC-B6L**) containing carbazole substituted thiophene moieties as an ancillary ligand were developed by Wu and co-workers [56]. The ε values of the MLCT band for both the dyes were enhanced compared with that of standard **N3** dye (Table 13). The cell η of the **53** (**CYC-B6S**) and **54** (**CYC-B6L**) dyes is higher than that of **N3** dye, under identical experimental conditions. Lower cell η of the **54** (**CYC-B6L**) dye compared with that of the **53** (**CYC-B6S**) is probably due to the different dye density on TiO$_2$ surface. Furthermore, the effect of the photostable hole-transporting carbazole moiety can be realized by the superior performances of both the dyes comparing with **36** (**CYC-B3**) dye.

The same group subsequently developed another dye, **55** (**CYC-B13**), which was similar to **53** (**CYC-B6S**), except that an EDOT group was introduced in the thiophene moiety [57]. Because an EDOT group was attached, the ε value of the lowest MLCT band of **55** (**CYC-B13**) is increased (Table 13), which provides superior J_{SC} of **55** (**CYC-B13**) when a thin-film device made of **55** (**CYC-B13**) dye was used and hence showed cell η augmentation along with higher stability compared with that of the **53** (**CYC-B6S**) dye, under identical conditions.

A "bithiophene-carbazole" antenna containing Ru sensitizer, **56** (**CYC-B7**), which is a homologue of **35** (**CYC-B1**) with a carbazole unit, was synthesized [58]. The $E_{1/2}^{Ru(III/II)}$ of the **56** (**CYC-B7**) dye was cathodically shifted by 40 mV, compared with the **35** (**CYC-B1**) dye, indicating that the carbazole unit destabilized the metal center. Concerning cell parameters, under identical conditions,

Table 12
Absorption data for entries **51**–**52**.

No	Code	λ_{max} (nm) (ε ($10^4 M^{-1} cm^{-1}$))[a]		Ref.
		π–π^* or dπ–π^*	dπ–π^*	
51	JK-55	354 (5.86) 470 (3.88)	539 (2.28)	[55]
52	JK-56	352 (3.59) 463 (2.44)	537 (1.84)	[55]

[a] In DMF.

Table 13
Absorption data for entries **53–55**.

No	Code	λ_{max} (nm) (ε (10^4 M^{-1} cm^{-1}))[a]		Ref.
		π–π^* or dπ–π^*	dπ–π^*	
53	**CYC-B6S**	401 (2.67)	548 (1.61)	[56]
54	**CYC-B6L**	400 (2.64)	551 (1.63)	[56]
55	**CYC-B13**	497 (–)	547 (1.93)	[57]

[a] In DMF.

except for the V_{OC} value, J_{SC}, FF and cell η values of **56** (**CYC-B7**) are inferior to that of the **35** (**CYC-B1**) dye. The lower J_{SC} and FF values are probably due to the molecular size and differences in dye density, along with an extensive H-aggregation of **56** (**CYC-B7**) on TiO$_2$ surface. However, the polarizability of **56** (**CYC-B7**) dye is higher than that of the **35** (**CYC-B1**) dye. This is due to the presence of a hole-transporting carbazole moiety, which causes an enhanced electric dipole moment of the dye-loaded titania film under an electric field and the resulting higher V_{OC} seen in the **56** (**CYC-B7**)-based DSC.

3.2. Ruthenium photosensitizers with 1,10-phenanthroline-based and dipyridylamine-based ancillary ligands

Ruthenium sensitizers having 1,10-phenanthroline (1,10-phen)- and dipyridylamine (DPA)-based ligands and the photovoltaic properties of the corresponding DSCs are given in Table 14.

Ruthenium dyes **57** (**AR20**) and **58** with 1,10-phen and dppz, respectively, as ancillary ligands were prepared by Kitao, Kasuga and co-workers [59]. The amount of dye **58** adsorbed on TiO$_2$ was higher than that of the **N719** and **57** (**AR20**) dyes. The higher adsorption for **58** can be attributed to the presence of a π-conjugated dppz ligand, which induced aggregate formation on the TiO$_2$ and prevented the transmission of light and hence the cell η value of **58** is lower than **57** (**AR20**).

The presence of strong electron-donating ($-$NH$_2$) or electron-withdrawing ($-$NO$_2$) substituents on the periphery of the 1,10-phen, enhanced the interfacial recombination between the e$^-$(TiO$_2$) and redox-active electrolyte (I$^-$/I$_3^-$) that limits the η, as have been observed with bpy based sensitizers [21]. Dyes **57** (**AR20** (H)) and **59–63** (**AR25** ($-$CH$_3$), **AR24** ($-$NH$_2$) and **AR27** ($-$NO$_2$)) were synthesized by Palomares and co-workers [60,61]. The ε of the MLCT band follows the order: **N719** $\approx$ **57** (**AR20**) > **60–61** (**AR24**) > **59** (**AR25**) > **62–63** (**AR27**) (Table 15). However, the efficiency of the electron injection from Dye$^{\bullet+}$ to the TiO$_2$ conduction band follows the order: **N719** (90%) $\approx$ **AR25** (90%) > **AR20** (85%) > **AR24** (70%) $\approx$ **AR27** and is consistent with a cell η order: **N719** $\approx$ **AR25** $\approx$ **AR20** > **AR24** $\approx$ **AR27**. Furthermore, two-fold faster CR between e$^-$(TiO$_2$)/electrolyte in **AR24** and **AR27** dyes dramatically lowers V_{OC} values, compared with the other dyes.

Wu and co-workers [62] synthesized two sensitizers **64** (**CYC-P1**) and **65** (**CYC-P2**), which contained the alkylthiophene-substituted 1,10-phen as an ancillary ligand. It should be noted that, though extending the conjugation lowers the MLCT energy, the ε value was less for both sensitizers, **64** (**CYC-P1**) and **65** (**CYC-P2**), compared with **N3** (Table 15). Electronic structure, as determined by semiempirical computations at the ZINDO/1 level, showed that although the HOMO and LUMO are localized on the Ru(II)-t$_{2g}$-NCS and dcbpy ligand, respectively, LUMO + 1 is largely localized on the ancillary ligand. The MLCT transition in **N3** dye involves dπ-Ru $\rightarrow$ dcbpy ligand, but in **64** (**CYC-P1**) and **65** (**CYC-P2**) dyes, a mixed dπ-Ru $\rightarrow$ dcbpy and ancillary ligand causes a low dipole moment for the transition and hence, a weak ε value. Furthermore, ancillary ligand does not connect to the TiO$_2$ surface and hence, decreases in the efficiency of the device.

A carbazole-functionalized phenanthrenyl-based Ru sensitizer **66** (**Ru-1**), along with two other dyes having phenyl **67** (**Ru-2**) and p-MeO-phenyl **68** (**Ru-3**) substituents were synthesized [63]. Among the three sensitizers, **66** (**Ru-1**) displayed better cell η properties owing to long-lived charge-separated state generated due to the presence of a carbazole unit along with high V_{OC} value [58].

Systematic studies concerning variation of the light-harvesting antennae from phenyl **69** (**JF-1**) – thiophene **70** (**JF-2**) – dithiophene **71** (**JF-5**) – linear trithiophene **72** (**JF-6**) – dendritic trithiophene **73** (**JF-7**) were developed by Lu and co-workers [64–66]. The **70** (**JF-2**) dye shows higher device η than that of the standard **N3** dye under identical conditions. This is due to the synergism of the enhanced light harvesting and directionality of the substitution which may increase the electric transition dipole moment of the dye-loaded TiO$_2$. The surface concentrations of the dyes on TiO$_2$ films and cell η follow the order: **70** (**JF-2**) > **N3** > **69** (**JF-1**) [64].

On traversing from the **70** (**JF-2**) to **71** (**JF-5**), **72** (**JF-6**) and **73** (**JF-7**), the trend for the ε value of MLCT band is in the order: **70** (**JF-2**) < **73** (**JF-7**) < **71** (**JF-5**) < **72** (**JF-6**) (Table 16). **72** (**JF-6**) contains three linear thiophene arrangements, while **73** (**JF-7**) contains bifurcated thiophene chains, resulting in a superior ε value for the MLCT band of the former. However, the elongation and/or bifurcation of the conjugated ancillary ligand decreases the quantity of the dye-loading on the TiO$_2$ surface (Γ), because of the larger volume of the dye molecules, a factor that lowers the device performance. A correlation between ε for the MLCT band I, Γ, and the device η of **70** (**JF-2**), **71** (**JF-5**), **72** (**JF-6**) and **73** (**JF-7**) is shown in Fig. 3.

Interestingly, plot of ε and Γ intersected around **71** (**JF-5**), resulting in the highest cell η among these dyes (Fig. 3). EIS data show that elongation and/or bifurcation of the conjugated ancillary ligand increases the resistance at the dye-adsorbed TiO$_2$/electrolyte interface together with a decrease in the electron transport in the TiO$_2$ network and follows the trend: **73** (**JF-7**) > **72** (**JF-6**) > **71** (**JF-5**). These are the reasons behind the η trend: **71** (**JF-5**) > **72** (**JF-6**) > **73** (**JF-7**) [65].

The electron-donating phenothiazine-based **74** (**JF-3**) and N,N-diphenylamino moiety substituted **75** (**JF-4**) Ru sensitizer have also been developed by Lu and co-workers. The ε of the MLCT band increased in the order: **74** (**JF-3**) > **70** (**JF-2**) > **75** (**JF-4**) [66]. In addition, **74** (**JF-3**) dye adsorbed onto TiO$_2$ film shows a broader
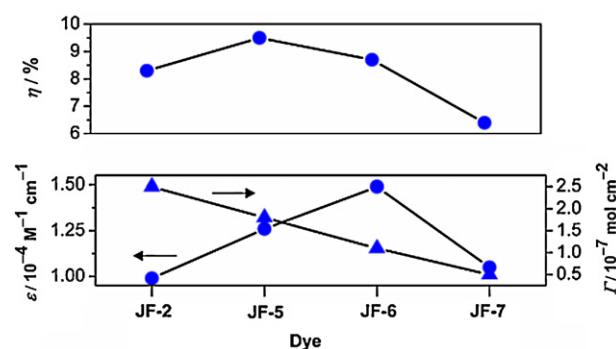

Fig. 3. Variation in the optical, dye-loading properties and power conversion efficiencies for **JF-2**, **JF-5**, **JF-6**, and **JF-7** [65].

Table 14
Molecular structures of ruthenium photosensitizers with various phenanthroline-based and dipyridylamine-based ancillary ligands and the photovoltaic properties of their corresponding DSCs.
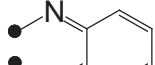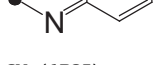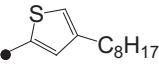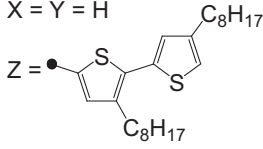
General formulas:
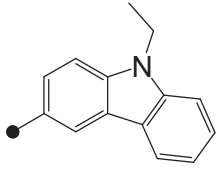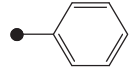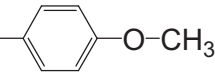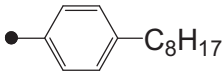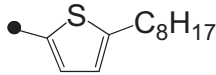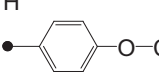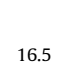
No	Substituent (Code)	J_{SC} (mA cm^{-2})	V_{OC} (V)	FF	η (%)	Ref.
57	X = Y = Z = H (**AR20**)	15.3	0.65	0.67	6.7[a]	[59]
58	X^1 ⋯ = X^2 ⋯	11.7	0.62	0.73	5.3[a]	[59]
59	Y = Z = H, X^1 = CH$_3$ (**AR25**)		0.69	0.39	2.6[b]	[60]
60	X^1 = H, X^2 = NH$_2$, Y = Z = H (**AR24a**)	0.2	0.48	0.31	0.2[c]	[61]
61	X^1 = X^2 = NH$_2$, Y = Z = H (**AR24b**)	0.1	0.46	0.31	0.1[c]	[61]
62	X^1 = H, X^2 = NO$_2$, Y = Z = H (**AR27a**)	0.8	0.44	0.34	0.8[c]	[61]
63	X^1 = X^2 = NO$_2$, Y = Z = H (**AR27b**)	0.1	0.44	0.35	0.1[c]	[61]
64	X = Y = H Z = (**CYC-P1**)	14.9	0.64	0.63	6.0[d]	[62]
65	X = Y = H Z = (**CYC-P2**)	9.8	0.55	0.64	3.4[d]	[62]
66	Q = C$_2$H$_5$, P = (**Ru-1**)	10.9	0.62	0.59	5.3[e]	[63]
67	Q = C$_2$H$_5$, P = (**Ru-2**)	7.7	0.48	0.64	3.1[e]	[63]
68	Q = C$_2$H$_5$ P = −O−CH$_3$ (**Ru-3**)	8.0	0.49	0.64	3.3[e]	[63]
69	Q = H, P = −C$_8$H$_{17}$ (**JF-1**)	12.9	0.78	0.69	6.9[f]	[64]
70	Q = H, P = (**JF-2**)	16.3	0.78	0.65	8.3[f]	[64]

Table 14 (*Continued*)

General formulas:

No	Substituent (Code)	J_{SC} (mA cm^{-2})	V_{OC} (V)	FF	η (%)	Ref.
71	Q = H, P = (**JF-5**)	18.3	0.73	0.71	9.5[g]	[65]
72	Q = H, P = (**JF-6**)	17.0	0.72	0.71	8.7[g]	[65]
73	Q = H, P = (**JF-7**)	13.1	0.70	0.70	6.4[g]	[65]
74	Q = H, P = (**JF-3**)	17.1	0.74	0.72	9.1[g]	[66]
75	Q = H, P = (**JF-4**)	16.1	0.71	0.69	7.9[g]	[66]
76	Q = H, P = (**Ru(Hipdpa)**)	18.7	0.63	0.58	6.8[h]	[67]
77	Q = H, P = (**Ru(Hpip)**)	7.8	0.55	0.60	2.5[h]	[67]

Table 14 (*Continued*)

General formulas:

No	Substituent (Code)	J_{SC} (mA cm^{-2})	V_{OC} (V)	FF	η (%)	Ref.
78	K = H, J = C$_{14}$H$_{29}$	15.5	0.76	0.70	8.2	[68]
79	K = H, J = (J13)	15.7	0.70	0.71	7.8[i]	[69]
80	K = H, J = (J16)	15.7	0.70	0.70	7.7[i]	[69]
81	J = C$_6$H$_{13}$, K = (JK-85)	16.5	0.71	0.65	7.7[j]	[70]
82	J = C$_6$H$_{13}$, K = (JK-86)	18.3	0.68	0.72	9.0[j]	[70]

● indicates the point of attachment of the substituent to the ancillary ligand.

[a] Under identical condition **N719** shows η = 8.8%.
[b] Under identical condition **N719** shows η = 3.6%.
[c] Under identical condition **N719** shows η = 4.4%.
[d] Under identical condition **N3** shows η = 7.7%.
[e] Under identical condition **N3** shows η = 6.0%.
[f] Under identical condition **N3** shows η = 8.1%.
[g] Under identical condition **N3** shows η = 8.8%.
[h] Under identical condition **N3** shows η = 6.5%.
[i] Under identical condition **N719** shows η = 7.9%.
[j] Under identical condition **N719** shows η = 8.9%.

visible spectrum coverage compared with that of the **70** (**JF-2**) and **75** (**JF-4**) dyes. This is because of the better planar configuration between thiophene and phenothiazine group. Also the slight bending butterfly conformation of the phenothiazine impedes molecular aggregation on the TiO$_2$ surface and the formation of intermolecular excimers. EIS data show that resistance at the interfacial recombination of the **74** (**JF-3**) sensitized solar cell is smaller and follows the trend: **75** (**JF-4**) > **70** (**JF-2**) > **74** (**JF-3**). Electron recombination lifetime in the TiO$_2$ films for **73** (**JF-3**) dye is 1.5 times greater than that of **75** (**JF-4**) dye and same to the **76** (**JF-2**) dye. The electron transport efficiency follows the trend: **75** (**JF-4**) ≈ **76** (**JF-2**) > **74** (**JF-3**) and is parallel to the cell η trend.

TPA functionalized phenanthrenyl-based Ru sensitizer **76** (**Ru(Hipdpa)**) was synthesized and its performance compared with phenyl substituted **77** (**Ru(Hpip)**) and **N3** dyes [67]. Upon the incorporation of the electron-donating TPA group, **76** (**Ru(Hipdpa)**) shows an 830 cm^{-1} red-shifted MLCT band with an enhanced ε value compared with **77** (**Ru(Hpip)**). As a consequence, **76**

(**Ru(Hipdpa)**) shows a superior device η than that of **77** (**Ru(Hpip)**). In fact, this is comparable with the **N3** dye, under identical conditions. In contrast to earlier reports [28,29], the study based on **76** (**Ru(Hipdpa)**) explained the inability of the TPA moiety to function as a HTM in Ru-complexes and, hence, the origin of the improved cell η by the introduction of the TPA unit required further explanation.

Grätzel, Zakeeruddin and co-workers [68] developed a heteroleptic ruthenium complex, **78**, containing dipyridylamine with a long alkyl chain as the ancillary ligand (DPA-R). DPA-R ligand has better σ-donor and poor π-acceptor properties, compared with bpy. The ε of the MLCT band (Table 17) and cell η value for the dye **78** are lower than those of the standard **N719** dye. The lower cell η value is due to CR of the e$^-$ (TiO$_2$) with the Dye$^{\bullet+}$ and slower dye regeneration compared with that of **N719** dye.

In an attempt to improve the ε value, the π-conjugation on the N-termini of the DPA-R ligand was extended. The triarylamine-functionalized Ru-dyes, **79** (**J13**) and **80** (**J16**) show cell η values

Table 15
Absorption and electrochemical data for entries **57–65**.

No	Code	λ_{max} (nm) (ε (10^4 M^{-1} cm^{-1}))[a]			E_{ox} of Ru(III/II) (V vs. SCE)[a]	Ref.
		$\pi-\pi^*$	$\pi-\pi^*$ or $d\pi-\pi^*$	$d\pi-\pi^*$		
57	AR20	267 (5.70)	309 (2.90) 400 (1.00)	492 (1.20)[b]	0.80	[59]
58		275 (5.70)	310 (3.50) 374 (1.80)	492 (1.10)[b]	0.83	[59]
59	AR25		423 (3.66)	518 (6.58)[c]	0.79	[60]
60	AR24a		420 (1.15)	546 (0.93)	0.75	[61]
61	AR24b		415 (1.04)	545 (0.93)	0.75	[61]
62	AR27a		403 (0.52)	538 (0.69)	0.72	[61]
63	AR27b		400 (0.49)	535 (0.66)	0.72	[61]
64	CYC-P1		302 (0.39) 380 (0.38)	518 (0.84)	0.78	[62]
65	CYC-P2		304 (0.28) 423 (0.22)	530 (0.38)	0.84	[62]

[a] In DMF.
[b] In 0.01 M NaOH.
[c] MeCN.

Table 16
Absorption and electrochemical data for entries **69–75**.

No	Code	λ_{max} (nm) (ε (10^4 M^{-1} cm^{-1}))[a]			E_{ox} of Ru(III/II) (V vs. SCE)[a]	Ref.
		$\pi-\pi^*$	$\pi-\pi^*$ or $d\pi-\pi^*$	$d\pi-\pi^*$		
69	JF-1	291 (5.46)	–	520 (1.09)	0.83	[64]
70	JF-2	298 (4.76)	358 (2.17)	519 (0.99)	0.86	[64]
71	JF-5	302 (3.59)	383 (3.95)	520 (1.26)	0.76	[65]
72	JF-6	299 (3.83)	417 (4.79)	520 (1.49)	0.78	[65]
73	JF-7	300 (4.87)	375 (2.75)	520 (1.05)	0.77	[65]
74	JF-3	298 (3.59)	342 (3.02)	520 (1.05)	0.81	[66]
75	JF-4	296 (4.95)	373 (1.56)	520 (1.02)	0.79	[66]

[a] In DMF.

similar to that of the **N719**, under identical conditions [69]. Density functional theory/time-dependent DFT studies predict that along with Ru(NCS) → dcbpy MLCT band, a substantial MLCT character on band at 380 nm, involving Ru(NCS) → TPA and dcbpy, and calculated spectra nicely reproduced experimental spectra of **78** (**J13**) and **79** (**J16**) dyes. Hence, efficient excited-state electron transfer occurred from the hole-transporting TPA moieties to the anchoring dcbpy ligand, which is attached to the TiO_2-surface.

Ko and co-workers [70] synthesized two amphiphilic heteroleptic ruthenium complexes that contained a *N*-alkyl substituted DPA ligand in which the 4,4′-positions were substituted with hexylthiophene **81** (**JK-85**) and hexylthienothiophene **82** (**JK-86**) ancillary ligands. The ε (Table 17) and η values follow the order: **82** (**JK-86**) > **N719** > **81** (**JK-85**). However, V_{OC} value follows the reverse order: **N719** > **81** (**JK-85**) > **82** (**JK-86**). This is related to the molecular size and intermolecular $\pi-\pi$ stacking interactions of the dyes. The electron lifetime is the smallest for **82** (**JK-86**) and hence, decreased dye coverage on TiO_2 resulted in a significant CR and lower V_{OC} value. Furthermore, in the dark, the resistance for the CR at the dyed TiO_2/electrolyte interface is lower for the **82** (**JK-86**) (63.35 Ω) than **81** (**JK-85**) (116.4 Ω) and **N719** (168.1 Ω), in accordance with the V_{OC} trend. Under illumination, the radius of the intermediate frequency semicircle in a Nyquist plot decreased

in the order: **81** (**JK-85**) > **82** (**JK-86**) ≈ **N719** and this indicates the improved charge generation and transport.

3.3. Ruthenium photosensitizers with modified anchoring ligands

In search of the next generation efficient light-harvesting antennae, anchoring ligand modified sensitizers have been developed (Table 18). For example, the 4,7-dicarboxy-1,10-phenanthroline (dcphen) containing Ru complex, **83**, shows one broad absorption with an enhanced ε value compared with the two MLCT bands seen in **N3** dye [71]. The $E_{1/2}^{Ru(III/II)}$ of the dye **83** is similar to that of the **N3** dye. Although with favorable light-harvesting properties, the J_{SC}, V_{OC} and cell η values of the [Bu_4N]$^+$ salt of **83** are lower than those of **N719** dye. Similarly, H_2dcbiq (**84**) and H_2dcdhph (**85**) anchoring ligand containing Ru sensitizers show encouraging absorption coverage up to near-infrared (NIR) region [72]. Despite better light harvesting, the cell η values of **84** and **85** are very low because of the inferior electron injection dynamics onto TiO_2 CB from Dye$^{•+}$, due to the low E_{ox}^* potential, which has been improved via the use of SnO_2 films. The lower device performance of the **83** compared with the **N3** dye could have followed the same explanation. A phenanthrenyl ligand containing Ru sensitizer **86** shows efficient

Table 17
Absorption and electrochemical data for entries **78–82**.

No	Code	λ_{max} (nm) (ε (10^4 M^{-1} cm^{-1}))			E_{ox} of Ru(III/II) (V vs. SCE)	Ref.
		$\pi-\pi^*$	$\pi-\pi^*$ or $d\pi-\pi^*$	$d\pi-\pi^*$		
78		317 (2.95)	426 (1.30)	568 (0.87)[a]	0.73[a]	[68]
79	J13	302 (–)	380 (–)	507 (–)[b]	–	[69]
80	J16	302 (–)	380 (–)	507 (–)[b]	–	[69]
81	JK-85		412 (1.82)	527 (1.02)[c]	0.79[d]	[70]
82	JK-86		418 (2.73)	525 (1.56)[c]	0.78[d]	[70]

[a] In 1:1 MeCN-^{t}BuOH.
[b] DMF.
[c] EtOH.
[d] MeCN.

Table 18
Photovoltaic properties for entries **83–102**.
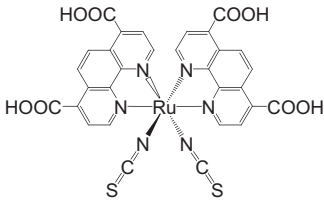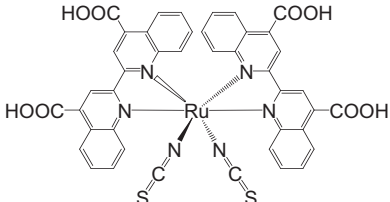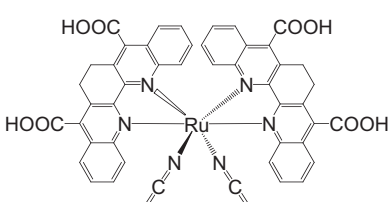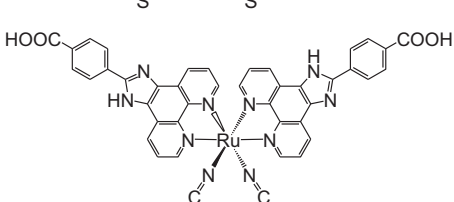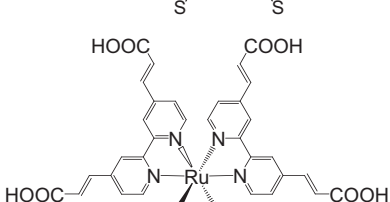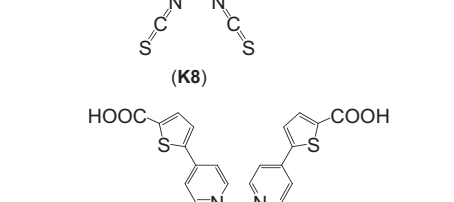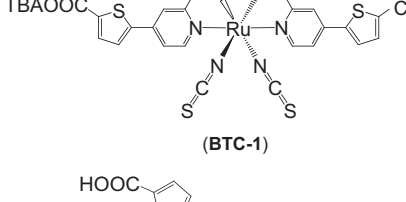
No	Substituent (code)	J_{SC} (mA cm^{-2})	V_{OC} (V)	FF	η (%)	Ref.
83		13.6	0.67	0.67	6.1[a]	[71]
84		0.8	0.50	0.72	0.3[b]	[72]
85		0.4	0.48	0.63	0.1[b]	[72]
86		0.1	0.57	0.49	0.3[c]	[73]
87	(**K8**)	18.0	0.64	0.75	8.6[d]	[74]
88	(**BTC-1**)	15.8	0.66	0.73	7.6[e]	[75]
89	(**BTC-2**)	16.1	0.75	0.74	9.1[f]	[76]

Table 18 (*Continued*)
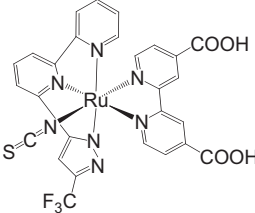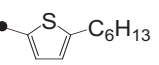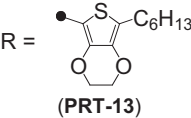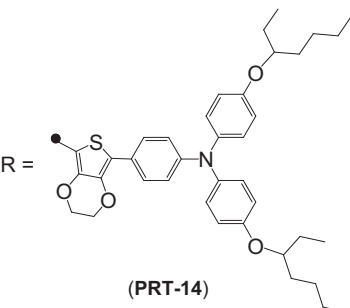
No	Substituent (code)	J_{SC} (mA cm^{-2})	V_{OC} (V)	FF	η (%)	Ref.
90		15.6	0.64	0.57	5.7[g]	[77]
91	X = H (**CK1**)	10.2	0.67	0.64	4.4[h]	[78]
92	X = COOH (**HY1**)	14.6	0.70	0.65	6.7[h]	[78]
93	X = H (**CK2**)	14.4	0.75	0.66	7.1[h]	[78]
94	X = COOH (**HY2**)	15.8	0.75	0.68	8.1[h]	[78]
95	R = H (**PRT-1**)	20.3	0.69	0.65	9.1[i]	[79]
96	R = OMe (**PRT-2**)	21.7	0.67	0.64	9.3[i]	[79]
97	R = OC$_8$H$_{17}$ (**PRT-3**)	20.4	0.72	0.65	9.6[i]	[79]
98	R = Bu^t (**PRT-4**)	21.6	0.71	0.65	10.1[i]	[79]
99	R = H (**PRT-11**)	13.5	0.68	0.73	6.7[j]	[80]
100	R = (thiophene)–C$_6$H$_{13}$ (**PRT-12**)	14.7	0.71	0.69	7.3[j]	[80]

Table 18 (*Continued*)

No	Substituent (code)	J_{SC} (mA cm^{-2})	V_{OC} (V)	FF	η (%)	Ref.
101	R = (PRT-13)	14.9	0.71	0.67	7.1[j]	[80]
102	R = (PRT-14)	16.3	0.75	0.68	8.3[j]	[80]

[a] 0.5 mM DMPII, 20 mM I$_2$, 0.5 M TBP, and 40 mM LiI in methoxyacetonitrile.
[b] 0.5 M DMPII, 0.03 M I$_2$, 0.5 M TBP, and 0.04 M LiI in methoxyacetonitrile.
[c] 0.5 M TBAI, 0.02 M LiI, 0.05 M I$_2$, and 0.5 M TBP in acetonitrile.
[d] 0.6 M methyl-*N*-butylimidazolium iodide, 0.05 M iodine, 0.05 M LiI, and 0.5 M TBP in a (1:1, v/v) mixture of valeronitrile and acetonitrile.
[e] 1.0 M DMII, 0.15 M I$_2$, 0.5 M, *n*-butylbenzimidazole, 0.1 M GuNCS in 3-methoxypropionitrile, under identical condition N719 shows η = 7.7%.
[f] 0.6 M DMII, 0.03 M I$_2$, 0.5 M TBP, 0.05 M LiI, and 0.1 M GuNCS in (85:15, v/v) acetonitrile:valeronitrile mixture, under identical condition Z907 shows η = 7.0%.
[g] 0.6 M butylmethylimidazolium iodide (BMII), 0.05 M I$_2$, 0.1 M LiI, 0.5 M TBP in (1:1, v/v) acetonitrile: valeronitrile mixture and 10% 3-methyl-2-oxazolidinone (NMO).
[h] 0.8 M 1-propyl-3-methylimidazolium iodide (PMII), 0.03 M I$_2$, 0.5 M TBP, and 0.13 M GuNCS in acetonitrile with 3×10^{-4} M deoxycholic acid (DCA) as a coadsorbate, under identical condition N719 shows η = 8.0%.
[i] 0.6 M dimethylpropylimidazolium iodide, 0.1 M I$_2$, 0.1 M LiI, and 0.5 M TBP in acetonitrile, under identical condition black dye shows η = 9.1%.
[j] 0.6 M dimethylpropylimidazolium iodide, 0.05 M I$_2$, 0.1 M LiI, and 0.5 M TBP in acetonitrile, under identical condition N749 shows η = 6.9%.

electron injection from Dye$^{\bullet+} \to$ TiO$_2$ CB resulting in comparable V_{OC} value of N3 dye. However, lesser dye adsorption on the surface of the TiO$_2$ photoanode and poor light harvesting lowers J_{SC} value with inferior cell η outcome of 86 [73].

A dcvbpy coordinated homoleptic ruthenium sensitizer, 87 (K8), was produced by Grätzel and co-workers [74]. A 50 mV cathodically shifted $E_{1/2}^{Ru(III/II)}$ value of 87 (K8) relative to that of the N3 dye is observed (Table 19) and this indicates the greater donor influence of a vinyl group in the 87 (K8) dye. Although the electron injection yield was lower by 10–20% for 87 (K8) relative to N3, this effect was compensated by the improved red absorbance of the former.

Another homoleptic Ru sensitizer, 88 (BTC-1), which contained a π-conjugated thiophene unit in the anchoring ligand was developed by Grätzel, Bäurele, and co-workers [75]. Because of enhancement in the ε value of MLCT absorption band, the J_{SC} is higher for 88 (BTC-1) compared with N719. Under identical conditions, 88 (BTC-1) shows superior cell η value compared with that of N719. However, when a scatter layer is added, the η value of both the dyes is similar.

A heteroleptic Ru sensitizer, 89 (BTC-2), is an analog of Z907 with a π-conjugated thiophene unit in the anchoring ligand (same as 88 (BTC-1)) [76]. The MLCT absorption band is 760 cm^{-1} red-shifted with simultaneous enhancement of ε value, compared with the standard Z907 dye. The $E_{1/2}^{Ru(III/II)}$ of 89 (BTC-2) dye is 60 mV cathodically shifted relative to Z907 dye, indicating a better electron-donating anchoring group because it contains a thiophene moiety. Under identical conditions, the J_{SC} as well as the cell η values of 89 (BTC-2) are higher compared with Z907 dye. Furthermore, the attachment of long alkyl chains provided better stability for the device with 89 (BTC-2), when subjected to light soaking at 60 °C for 1000 h.

Chou, Chi and co-workers [77] developed heteroleptic Ru sensitizers with a monoanionic tridentate pyrazole substituted 2,2′-bipyridine ligand. The sensitizer 90, had a lower cell η value than that for the N3 dye. In order to improve device efficiency, they varied the carboxylic acid group(s) on the anchoring ligand

as well as the π-conjugation in the ancillary ligand to generate the Ru sensitizers [78], 91 (CK1), 92 (HY1), 93 (CK2), and 94 (HY2). The ε value of the MLCT band enhanced with increasing conjugation on the ancillary ligand and follows the order: 91 (CK1) < 92 (HY1) < 93 (CK2) < 94 (HY2) (Table 20). The trend for device η values is the same as the trend for ε values. Due to low ε values, the 91 (CK1) and 92 (HY1) dyes show lower cell η values, compared with the N719 dye. Among the 93 (CK2) and 94 (HY2) dyes, the lower η value of the 93 (CK2) dye is due to a lower dye uptake because of the presence of a single —COOH group vs. two —COOH in the case of the 94 (HY2) dye and the cell η value for the 94 (HY2) dye is comparable to that for the N719 dye.

A series of neutral Ru(II) terpyridine sensitizers 95–98 (PRT1–PRT4) were synthesized [79]. Compared with the black dye, they exhibited a high absorption in the 420–520 nm region with onset on the NIR region. In this series, 98 (PRT4) exhibited higher efficiency and the cell η value increased compared with the parent black dye. All the dyes show enhanced photostability due to chelation configuration.

Chou, Chi and co-workers [80] recently developed a series of tris(thiocyanate)ruthenium photosensitizers, having a functionalized tridentate ligand with two carboxy groups 99–102 (PRT-11–PRT-14). Several electron-donating substituents, such as hexylthiophene 100 (PRT-12), hexyl-EDOT 101 (PRT-13) and a functionalized-TPA 102 (PRT-14) were introduced at the third carboxy-free pyridine moiety. Among the four sensitizers, 102 (PRT-14) showed an enhanced hyperchromic effect due to the presence of the TPA moiety (Table 21), which increases donor–acceptor coupling and hence the corresponding transition dipole.

3.4. Thiocyanate-free ruthenium photosensitizers

In an attempt to replace the thiocyanate moiety, which makes the chemical stability of the ruthenium sensitizer vulnerable, thiocyanate-free cyclometalated ruthenium sensitizers were

Table 19
Absorption and electrochemical data for entries **87**–**89**.

No	Code	λ_max (nm) (ε (10⁴ M⁻¹ cm⁻¹))[a]			E_ox of Ru(III/II) (V vs. SCE)[a]	Ref.
		π–π*	π–π* or dπ–π*	dπ–π*		
87	**K8**	312 (–)	326 (–) 439 (–)	555 (–)	0.79	[74]
88	**BTC-1**	287 (5.90)	331 (6.23) 426 (2.48)	563 (2.32)	0.73	[75]
89	**BTC-2**	299 (5.75)	341 (3.37) 422 (1.62)	548 (1.60)	0.64	[76]

[a] In DMF.

Table 20
Absorption data for entries **90**–**94**.

No	Code	λ_max (nm) (ε (10⁴ M⁻¹ cm⁻¹))[a] dπ–π*	Ref.
90		520 (1.30)	[77]
91	**CK1**	517 (0.88)	[78]
92	**HY1**	521 (1.04)	[78]
93	**CK2**	541 (1.83)	[78]
94	**HY2**	550 (1.98)	[78]

[a] In DMF.

synthesized (Table 22) [81]. Cyclometalation, the replacement of a neutral heteroatom with an isoelectronic anionic carbon center in a multidentate ligand containing additional heteroatoms, allows the tuning of redox potentials and electronic properties of the complexes. Grätzel and co-workers [82] reported a cyclometalated ruthenium sensitizer, **104**. The lowest energy MLCT band of the sensitizer, when compared with **N719** dye, was red-shifted by 830 cm⁻¹ along with the appearance of a new band at 490 nm with a higher ε value. The Ru(II)–C σ-bond formation reflects on the 40 mV cathodically shifted $E_{1/2}^{Ru(III/II)}$ potential from that of **N719** dye. The η value of the sensitizer is >10% and was lower when the fluorine is not present in the cyclometalated ligand. The presence of fluorine reduces the electron-donating behavior of the cyclometalating ligand as well as reduces Lewis basicity. This stabilizes the Ru(III) oxidation state which may allow easy dye regeneration and efficient electron injection [82].

Ruthenium sensitizers **105**–**107** (**TFRS-1**–**TFRS-3**), free of thiocyanate ligands, were synthesized with pypz ancillary ligands [83]. As expected, upon extending the π-conjugation of the backbone of the pyridyl-pyrazolate chelates, the ε value increased on traversing from **105** (**TFRS-1**) → **106** (**TFRS-2**) → **107** (**TFRS-3**) and J_SC follows the same trend. The V_OC and cell η values of **105** (**TFRS-1**) are higher than the standard **N719** dye, indicating that the pyridyl-pyrazolate chelate is a better insulator than –SCN which blocks the dark current and enhanced V_OC. However, the V_OC values for **106** (**TFRS-2**) and **107** (**TFRS-3**) were lower than the parent dye, due to their large molecular size resulting in a lower dye density and also defective packing, giving rise to an increase in dark current. Furthermore, EIS data in the dark revealed that the CR kinetics are slower for **TFRS** dyes than for the **N719** dye, and **106** (**TFRS-2**) showed the best performance, with higher cell η than **N719**.

Chi, Chou and co-workers [84] synthesized a series of thiocyanate-free bis-tridentate (pyridyl bis-pyrazolate chelates,

bpzpy) ancillary ligand and tricarboxyterpyridine anchoring ligand containing Ru-photosensitizers, **108**–**111** (**TF-1**–**TF-4**). The use of dual tridentate ligand adds more stability and, also prevents thiocyanate isomerism. The dyes cover the entire visible range (Table 23), with a shoulder extending up to 800 nm with enhanced ε values compared with the standard **N749** or black dye. As a consequence, the J_SC values of all **TF**-dyes are superior to the **N749** dye. All the dyes exhibit favorable HOMO and LUMO energy levels for electron injection and regeneration. The CR dynamics of these dyes are slower than **N749** dye and resulting in V_OC differences as high as 70 mV between the **109** (**TF-2**) and **N749** dyes. Devices made with these dyes displayed good cell η values, with **110** (**TF-3**) exhibiting an efficiency that was higher than **N749** dye.

To investigate the influence of cyclometalation (N,N′,N″ vs. N,C,N′ vs. C,N,N′) on the sensitizing properties of dyes, van Koten and co-workers [85] reported on the elegant preparation of some cyclometalated ruthenium sensitizers **112**–**114** (Table 22). The absorption spectra of the cyclometalated ruthenium sensitizers showed broadening and red-shift, accompanied by a cathodically shifted $E_{1/2}^{Ru(III/II)}$ compared with that of [Ru(tpy)₂]²⁺. In **112**, excited state does not possess appropriate energy ordering and also electron density in the lowest excited state is localized in a remote terpyridine moiety as determined by the time-dependent DFT calculations. These two factors cause inefficient injection of electrons from the excited state of **112** into the TiO₂ conduction band. This in contrast to dye **113**, in which the electron density is largely localized in the C–H activated C,N,N′ ligand in the excited state and thus, electron injection to TiO₂ becomes more efficient. Furthermore, dye **114** contains an additional –COOH group as well, which results in the further lowering of the LUMO energy level with additional electron density largely localized in the C,N,N′ ligand in the excited state.

Berlinguette and co-workers [86–88] comprehensively studied bis-tridentate (TPA-attached tridentate ancillary ligand and tricarboxyterpyridine anchoring ligand) cyclometalated ruthenium complexes (selected sensitizers (**115**–**118**) are shown in Table 22). When the Ru–N bond was replaced with an anionic Ru–C bond using a cyclometalating ligand, the degeneracy of the frontier orbitals are lowered and thus MLCT and ILCT transitions are separated to give a broad absorption profile, instead of an intense absorption, such as that seen in polypyridyl complexes. Furthermore, the anionic ligand induces a red-shift in the MLCT transition, because the tpy-based π* orbitals are raised to higher energies to a lesser extent than the metal-based t₂g orbitals. They also observed

Table 21
Absorption and electrochemical data for entries **99**–**102**.

No	Code	λ_max (nm) (ε (10⁴ M⁻¹ cm⁻¹))[a]			E_ox of Ru(III/II) (V vs. SCE)[b]	Ref.
		π–π*	π–π* or dπ–π*	dπ–π*		
99	**PRT-11**	324 (1.95)	393 (0.64)	521 (0.43) 579 (0.57)	0.84	[80]
100	**PRT-12**	310 (1.39)	368 (2.37)	600 (0.37)	0.85	[80]
101	**PRT-13**	316 (1.89)	389 (2.95)	535 (0.40) 600 (0.50)	0.85	[80]
102	**PRT-14**	309 (2.82)	362 (2.88) 475 (3.33)	600 (0.74)	0.86	[80]
	N749	326 (2.16)	339 (2.22), 403 (0.96)	522 (0.48) 600 (0.68)	0.89	[80]

[a] In MeOH.
[b] In DMF.

Table 22
Photovoltaic parameters for entries **103–118**.
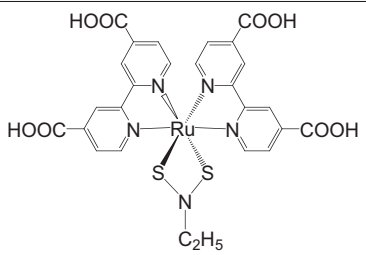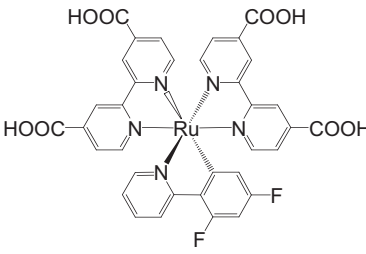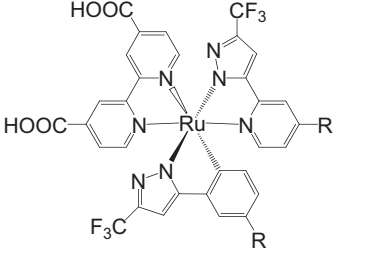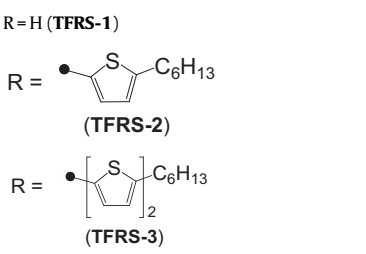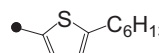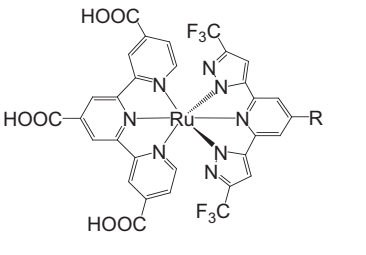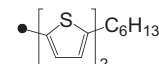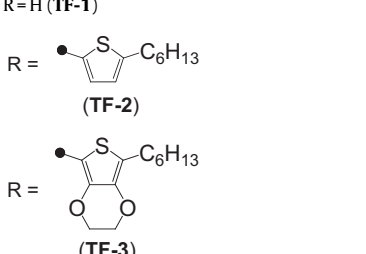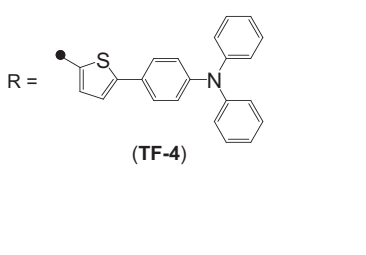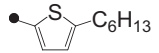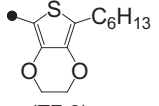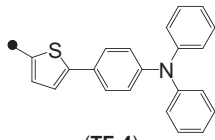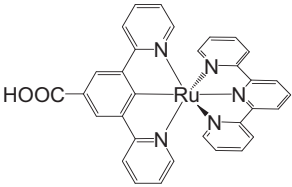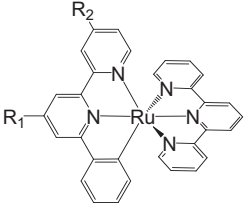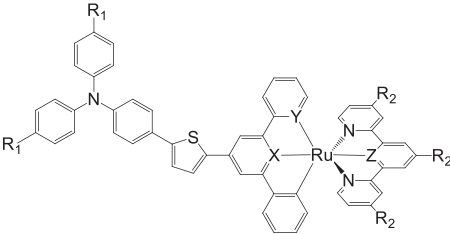
No	Substituent (code)	J_{SC} (mA cm^{-2})	V_{OC} (V)	FF	η (%)	Ref.
103		–	–	–	–	[81]
104		17.0	0.80	0.74	10.1[a]	[82]
105	R = H (**TFRS-1**)	15.9	0.83	0.69	9.2[a,b]	[83]
106	R = (**TFRS-2**)	17.1	0.82	0.68	9.5[a,b]	[83]
107	R = (**TFRS-3**)	17.4	0.81	0.63	8.9[a,b]	[83]
108	R = H (**TF-1**)	18.2	0.74	0.68	9.1[c]	[84]
109	R = (**TF-2**)	20.0	0.79	0.67	10.5[c]	[84]
110	R = (**TF-3**)	21.4	0.76	0.66	10.7[c]	[84]
111	R = (**TF-4**)	20.3	0.77	0.67	10.5[c]	[84]

Table 22 (*Continued*)

No	Substituent (code)	J_{SC} (mA cm^{-2})	V_{OC} (V)	FF	η (%)	Ref.
112						[85]
113	R1 = COOH, R2 = H					[85]
114	R1, R2 = COOH					[85]
115	X = N, Y = C, Z = N, R$_1$ = H, R$_2$ = COH	14.9	0.67	0.71	7.1	[86]
116	X = C, Y = N, Z = N, R$_1$ = Me, R$_2$ = CO$_2$H	8.3	0.61	0.77	3.9	[86]
117	X = N, Y = C, Z = N, R$_1$ = Me, R$_2$ = CO$_2$H	13.0	0.65	0.75	6.3	[86]
118	X = N, Y = C, Z = N, R$_1$ = OMe, R$_2$ = CO$_2$H	16.7	0.68	0.71	8.0	[86]

[a] 0.6 M butylmethylimidazolium iodide (BMII), 0.1 M GuNCS, 0.03 M I$_2$, and 0.5 M TBP in (85:15, v/v) acetonitrile: valeronitrile mixture.
[b] Under identical condition **N719** shows η = 8.6%.
[c] 0.6 M dimethylpropylimidazolium iodide, 0.1 M I$_2$, 0.1 M LiI, and 0.5 M TBP in acetonitrile, under identical condition **N749** shows η = 9.2%.

that the intensity of the absorption spectra in the visible region is enhanced, when the M—C bond is orthogonal to the principal axis. Devices made with cyclometalated ruthenium sensitizers **115–118** exhibited η values in the range from 3.9 to 8%.

3.5. Other ruthenium sensitizers

A sensitizer that covers a large part of the visible spectrum is essential for efficient light harvesting and the conversion of solar energy. Structural modifications, by means of geometrical isomerization, can result in an extended absorption up to the NIR region [89,90]. The *trans* isomer of the **N3** complex, in which the two thiocyanate ligands are in a *trans* arrangement, shows sensitivity in the NIR region, whereas the *cis* isomer has no absorption in that region [91]. However, the limitation of the *trans* isomer is that it undergoes thermal or photochemical isomerization to the *cis*-form.

Grätzel and co-workers [91] synthesized a ruthenium complex, **119** (**N886**), with a tetradentate ligand, and the two thiocyanate

ligands were in a *trans* configuration (Table 24). The strategy for using the tetradentate ligand was to stabilize the *trans* geometry of the molecule. The absorption features of **119** (**N886**) were extended up to the NIR region (Table 25). When compared with the MLCT band of **N719** dye, it is red-shifted by 3170 cm^{-1}, however, ε of this band is lower for the **119** (**N886**) dye, resulting in a low J_{SC} value. The V_{OC} value of **119** (**N886**) dye is 120 mV lower than **N719** dye, as the excited states of **119** (**N886**) dye were not properly oriented relative to the conduction band of TiO$_2$ and aggregation of the dye occurred as well, and thus, showed a low cell η value.

Very recently, the heteroarylvinylene π-conjugated quaterpyridine-based ruthenium sensitizer, **120** (**N1044**) was reported [92] (Table 24). The introduction of an EDOT moiety, along with π-conjugation, results in the entire visible region being covered, with a strong absorption in the 400–450 nm region. Compared with the *t*-butyl substituted **119** (**N886**) dye, the ε value at ~400 nm was enhanced and the $E_{1/2}^{Ru(III/II)}$ value was 90 mV cathodically shifted. The HOMO energy level was

Table 23
Absorption and electrochemical data for entries **108–111**.

No	Code	λ_{max} (nm) (ε (10^4 M^{-1} cm^{-1}))[a]				E_{ox} of Ru(III/II) (V vs. SCE)[a]	Ref.
		π–π^*	π–π^* or dπ–π^*	dπ–π^*	dπ–π^*+L–L[b]		
108	**TF-1**	318 (2.49)	383 (0.91) 417 (0.85)	510 (0.91)	640 (0.16) 721 (0.17)	0.70	[84]
109	**TF-2**	329 (4.79)	421 (1.84)	509 (1.92)	654 (0.25) 719 (0.24)	0.71	[84]
110	**TF-3**	322 (5.16)	387 (1.88) 426 (2.20)	513 (2.19)	653 (0.27) 723 (0.26)	0.73	[84]
111	**TF-4**	333 (3.90)	404 (3.24) 447 (2.93)	516 (3.09)	662 (0.23) 716 (0.23)	0.70	[84]

[a] In DMF.
[b] Ligand-to-ligand charge transfer.

Table 24
Photovoltaic parameters for entries **119–126**.
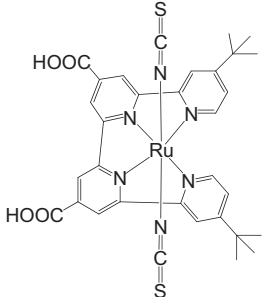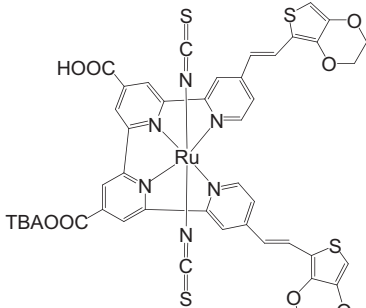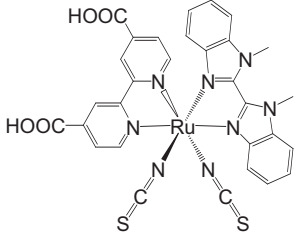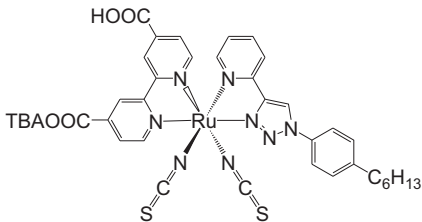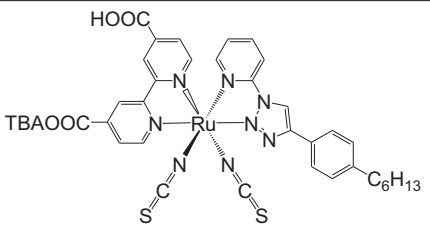
No	Substituent (Code)	J_{SC} (mA cm^{-2})	V_{OC} (V)	FF	η (%)	Ref.
119	(**N886**)	11.8	0.68	0.73	5.9[a]	[91]
120	(**N1044**)	19.1	0.45	0.67	5.7[b]	[92]
121	R = Me (**RD1**)	12.7	0.69	0.68	6.0[c]	[93]
122	R = C$_{10}$H$_{21}$ (**RD10**)	13.6	0.71	0.70	6.8[c]	[93]
123	R = benzyl (**RD5**)	15.1	0.74	0.69	7.7[c]	[93]
124	(**RD11**)	11.2	0.69	0.67	5.1[c]	[93]
125		13.2	0.76	0.77	7.8[d]	[94]

Table 24 (Continued)

No	Substituent (Code)	J_{SC} (mA cm^{-2})	V_{OC} (V)	FF	η (%)	Ref.
126		8.9	0.67	0.77	4.7[d]	[94]

[a] 0.60 M 1-propyl-3-methylimidazolium iodide, 0.03 M I$_2$, 0.5 M TBP, in (1:1, v/v) mixture of acetonitrile and valeronitrile.

[b] 0.6 M butylmethylimidazolium iodide (BMII), 0.05 M I$_2$, 0.1 M LiI, in (85:15, v/v) acetonitrile: valeronitrile mixture.

[c] 1.0 M butylmethylimidazolium iodide (BMII), 0.1 M GuNCS, 0.03 M I$_2$, 0.05 M LiI, and 0.5 M TBP in (85:15, v/v) acetonitrile:valeronitrile mixture.

[d] 1.0 M DMII, 0.03 M I$_2$, 0.5 M TBP, and 0.1 M GuNCS in (85:15, v/v) acetonitrile:valeronitrile mixture.

Table 25
Absorption and electrochemical data for entries **119**–**120**.

No	Code	λ_{max} (nm) (ε (10^4 M^{-1} cm^{-1}))[a]		E_{ox} of Ru(III/II) (V vs.SCE)[a]	Ref.
		π–π^*	$d\pi$–π^*		
119	**N886**	333 (2.12) 395 (1.03)	543 (0.74) 649 (0.83)	0.53	[92]
120	**N1044**	298 (3.20) 400 (3.55)	615 (0.75)	0.44	[92]

[a] In DMF.

destabilized by 0.1 and 0.2 eV compared with the **119** (**N886**) and **N719** (also **38** (**Ru-EDOT**)) dyes, respectively, and HOMO–LUMO energy gap follows the decreasing order: **38** (**Ru-EDOT**) > **119** (**N886**) ≈ **N719** > **120** (**N1044**). Despite the favorable properties of the **120** (**N1044**) dye, the cell η value was lower compared with the standard **N719** dye. This is mainly due to the lower V_{OC}, which can be explained as follows: (i) loose packing of dye that allowed CR between e$^-$(TiO$_2$) and the oxidized electrolyte; (ii) the HOMO of **120** (**N1044**) dye lies close to the TiO$_2$ surface, does not form an insulating barrier towards CR between the injected electron and the Dye$^{•+}$.

Diau and co-workers [93], in an effort to easily prepare ruthenium sensitizers, synthesized benzimidazole-based ruthenium sensitizers and investigated their light to electrical energy conversion properties. They utilized four different substituted benzimidazoles and generated four ruthenium sensitizers **121** (**RD1**), **122** (**RD10**), **123** (**RD5**), **124** (**RD11**) (Table 24). Among these four sensitizers, **123** (**RD5**) showed a better absorption and had a higher J_{SC}, and owing to mitigated recombination dynamics, it had an increased V_{OC} relative to the others.

Grätzel, Bäuerle and co-workers [94] utilized a click-chemistry approach to synthesize 1,2,3-triazolylpyridine ligands and the corresponding Ru sensitizers **125**, **126** were reported. The dyes showed a diminished absorption compared with other standard Ru dyes [10,50,75,89]. The position of the substituents influenced the performance of sensitizers **125** and **126**: the former exhibited better efficiency relative to the latter, owing to a higher absorption and decreased recombination.

4. Concluding remarks

Strategies applied in the designing of various classes of ruthenium dyes employed in DSCs and their structure – photophysical and electrochemical properties – photovoltaic parameters are correlated in this review. The different approaches adopted to enhance light harvesting, extend the absorption in the NIR region in ruthenium dyes, improve the stability of the dyes, and interfacial CR dynamics have been presented. All these aspects will be helpful in an understanding and appreciation of those dyes, which can serve as a guide for the design of the next generation of efficient

photosensitizers for realizing sustainable energy. We believe that the information provided in this review will be a significant asset for the steadily growing number of dye designers who wish to have a one-stop look at the other successful dyes and design strategies developed in the last 20 years.

Notwithstanding the brilliant progress made to date, the best-performing modern ruthenium DSCs are surprisingly similar to the conventional "Grätzel Cell" [9]. It is most likely that other classes of photosensitizing coordination compounds with transition metals such as, Fe(II) [95], Pt(II) [96], Re(I) [97], Ir(III) [98], and donor-π-bridge-acceptor dyes [99,100] will be available in view of the preliminary promising results that have been appeared recently. To summarize, more ingenious organic ligands for the development of functional metal complexes continue to hold promise regarding the development of "efficient dye-sensitized solar cells".

References

[1] International Energy Outlook 2010, Energy Information Administration, (2010) http://www.eia.gov/oiaf/ieo/index.html.
[2] M.I. Hoffert, K. Caldeira, A.K. Jain, E.F. Haites, L.D.D. Harvey, S.D. Potter, M.E. Schlesinger, S.H. Schneider, R.G. Watts, T.M.L. Wigley, D.J. Wuebbles, Nature 395 (1998) 881.
[3] K.S. Deffeyes, Beyond Oil, the View from Hubbert's Peak, Hill and Wang, New York, 2005.
[4] V. Smil, Energy at the Crossroads, Global Perspectives and Uncertainties, MIT Press, Cambridge, 2003.
[5] http://www.wbgu.de/.
[6] N.S. Lewis, Science 315 (2007) 798.
[7] Basic Research Needs for Solar Energy Utilization, BES Workshop on Solar Energy Utilization, April 18–25, 2005.
[8] M. Grätzel, Acc. Chem. Res. 42 (2009) 1788.
[9] B. O'Regan, M. Grätzel, Nature 353 (1991) 737.
[10] M.K. Nazeeruddin, A. Key, L. Rodicio, R. Humphrey-Baker, E. Müller, P. Liska, N. Vlachopoulos, M. Grätzel, J. Am. Chem. Soc. 115 (1993) 6382.
[11] A.B.F. Martinson, T.W. Hamann, M.J. Pellin, J.T. Hupp, Chem. Eur. J. 14 (2008) 4458.
[12] Y. Luo, D. Li, Q. Meng, Adv. Mater. 21 (2009) 4647.
[13] M.K. Nazeeruddin, S.M. Zakeeruddin, R. Humphry-Baker, M. Jirousek, P. Liska, N. Vlachopoulos, V. Shklover, C.-H. Fischer, M. Grätzel, Inorg. Chem. 38 (1999) 6298.

[14] M.K. Nazeeruddin, P. Péchy, T. Renouard, S.M. Zakeeruddin, R. Humphrey-Baker, P. Comte, P. Liska, L. Cevey, E. Costa, V. Shklover, L. Spiccia, G.B. Deacon, C.A. Bignozzi, M. Grätzel, J. Am. Chem. Soc. 123 (2001) 1613.

[15] X. Li, K. Hou, X. Duan, F. Li, C. Huang, Inorg. Chem. Commun. 9 (2006) 394.

[16] M.K. Nazeeruddin, S.M. Zakeeruddin, J.-J. Lagref, P. Liska, P. Comte, C. Barolo, G. Viscardi, K. Schenk, M. Grätzel, Coord. Chem. Rev. 248 (2004) 1317.

[17] J.E. Kroeze, N. Hirata, S. Koops, M.K. Nazeeruddin, L. Schmidt-Mende, M. Grätzel, J.R. Durrant, J. Am. Chem. Soc. 128 (2006) 16376.

[18] S.M. Zakeeruddin, M.K. Nazeeruddin, R. Humphry-Baker, P. Péchy, P. Quagliotto, C. Barolo, G. Viscardi, M. Grätzel, Langmuir 18 (2002) 952.

[19] L. Schmidt-Mende, J.E. Kroeze, J.R. Durrant, M.K. Nazeeruddin, M. Grätzel, Nano Lett. 5 (2005) 1315.

[20] W.-S. Han, J.-K. Han, H.-Y. Kim, M.J. Choi, Y.-S. Kang, C. Pac, S.O. Kang, Inorg. Chem. 50 (2011) 3271.

[21] P. Wang, S.M. Zakeeruddin, J.E. Moser, M.K. Nazeeruddin, T. Sekiguchi, M. Gratzel, Nat. Mater. 2 (2003) 402.

[22] P. Wang, S.M. Zakeeruddin, J.E. Moser, R. Humphrey-Baker, P. Comte, V. Aranyos, A. Hagfeldt, M.K. Nazeeruddin, M. Grätzel, Adv. Mater. 16 (2004) 1806.

[23] P. Wang, C. Klein, R. Humphrey-Baker, S.M. Zakeeruddin, M. Grätzel, J. Am. Chem. Soc. 127 (2005) 808.

[24] D. Kuang, C. Klein, S. Ito, J.E. Moser, R. Humphrey-Baker, N. Evans, F. Duriaux, C. Grätzel, S.M. Zakeeruddin, M. Grätzel, Adv. Mater. 19 (2007) 1133.

[25] D. Kuang, S. Ito, B. Wenger, C. Klein, J.-E. Moser, R. Humphry-Baker, S.M. Zakeeruddin, M. Grätzel, J. Am. Chem. Soc. 128 (2006) 4146.

[26] M.K. Nazeeruddin, Q. Wang, L. Cevey, V. Aranyos, P. Liska, E. Figgemeier, C. Klein, N. Hirata, S. Koops, S.A. Haque, J.R. Durrant, A. Hagfeldt, A.B.P. Lever, M. Grätzel, Inorg. Chem. 45 (2006) 787.

[27] C. Klein, M.K. Nazeeruddin, D.D. Censo, P. Liska, M. Grätzel, Inorg. Chem. 43 (2004) 4216.

[28] A.J. Hallett, J.E. Jones, Dalton Trans. 40 (2011) 3871.

[29] F. Matar, T.H. Ghaddar, K. Walley, T. DosSantos, J.R. Durrant, B. O'Regan, J. Mater. Chem. 18 (2008) 4246.

[30] D. Kuang, C. Klein, H.J. Snaith, J.-E. Moser, R. Humphrey-Baker, P. Comte, S.M. Zakeeruddin, M. Grätzel, Nano Lett. 6 (2006) 769.

[31] H.J. Snaith, S.M. Zakeeruddin, L. Schmidt-Mende, C. Klein, M. Grätzel, Angew. Chem. Int. Ed. 44 (2005) 6413.

[32] J. Krüger, U. Bach, M. Grätzel, Adv. Mater. 12 (2000) 447.

[33] D. Kuang, C. Klein, S. Ito, J.-E. Moser, R. Humphrey-Baker, S.M. Zakeeruddin, M. Grätzel, Adv. Funct. Mater. 17 (2007) 154.

[34] N. Lu, J.-S. Shing, W.-H. Tu, Y.-C. Hsu, J.T. Lin, Inorg. Chem. 50 (2011) 4289.

[35] C. Lee, J.-H. Yum, H. Choi, S.O. Kang, J. Ko, R. Humphry-Baker, M. Grätzel, M.K. Nazeeruddin, Inorg. Chem. 47 (2008) 2267.

[36] H.J. Snaith, C.S. Karthikeyan, A. Petrozza, J. Teuscher, J.E. Moser, M.K. Nazeeruddin, M. Thelakkat, M. Grätzel, J. Phys. Chem. C 112 (2008) 7562.

[37] J.-H. Yum, I. Jung, C. Baik, J. Ko, M.K. Nazeeruddin, M. Grätzel, Energy Environ. Sci. 2 (2009) 100.

[38] N. Hirata, J.J. Lagref, E.J. Palomares, J.R. Durrant, M.K. Nazeeruddin, M. Grätzel, D.D. Censo, Chem. Eur. J. 10 (2004) 595.

[39] S.A. Haque, S. Handa, K. Peter, E. Palomares, M. Thelakkat, J.R. Durrant, Angew. Chem. Int. Ed. 44 (2005) 5740.

[40] S.-R. Jang, C. Lee, H. Choi, J.J. Ko, J. Lee, R. Vittal, K.-J. Kim, Chem. Mater. 18 (2006) 5604.

[41] K.-J. Jiang, N. Masaki, J.-b. Xia, S. Noda, S. Yanagida, Chem. Commun. (2006) 2460.

[42] C.-Y. Chen, S.-J. Wu, C.-G. Wu, J.-G. Chen, K.-C. Ho, Angew. Chem. Int. Ed. 45 (2006) 5822.

[43] C.-Y. Chen, S.-J. Wu, J.-Y. Li, C.-G. Wu, J.-G. Chen, K.-C. Ho, Adv. Mater. 19 (2007) 3888.

[44] A. Abbotto, C. Barolo, L. Bellotto, F.D. Angelis, M. Grätzel, N. Manfredi, C. Marinzi, S. Fantacci, J.H. Yum, M.K. Nazeeruddin, Chem. Commun. (2008) 5318.

[45] J.N. Clifford, E. Palomares, M.K. Nazeeruddin, M. Grätzel, J.R. Durrant, J. Phys. Chem. C 111 (2007) 6561.

[46] C.-Y. Chen, M. Wang, J.-Y. Li, N. Pootrakulchote, L. Alibabaei, C.-h. Ngoc-le, J.-D. Decoppet, J.-H. Tsai, C. Grätzel, C.-G. Wu, S.M. Zakeeruddin, M. Grätzel, ACS Nano 3 (2009) 3103.

[47] F. Gao, Y. Wang, D. Shi, J. Zhang, M. Wang, X. Jing, R. Humphry-Baker, P. Wang, S.M. Zakeeruddin, M. Grätzel, J. Am. Chem. Soc. 130 (2008) 10720.

[48] F. Gao, Y. Wang, J. Zhang, D. Shi, M. Wang, R. Humphry-Baker, P. Wang, S.M. Zakeeruddin, M. Grätzel, Chem. Commun. (2008) 2635.

[49] Q. Yu, S. Liu, M. Zhang, N. Cai, Y. Wang, P. Wang, J. Phys. Chem. C 113 (2009) 14559.

[50] F. Gao, Y. Cheng, Q. Yu, S. Liu, D. Shi, Y. Li, P. Wang, Inorg. Chem. 48 (2009) 2664.

[51] Y. Cao, Y. Bai, Q. Yu, Y. Cheng, S. Liu, D. Shi, F. Gao, P. Wang, J. Phys. Chem. C 113 (2009) 6290.

[52] F. Sauvage, M.K.R. Fischer, A. Mishra, S.M. Zakeeruddin, M.K. Nazeeruddin, P. Bäuerle, M. Grätzel, ChemSusChem 2 (2009) 761.

[53] X. Lv, F. Wang, Y. Li, ACS Appl. Mater. Interfaces 2 (2010) 1980.

[54] J.-J. Kim, K. Lim, H. Choi, S. Fan, M.-S. Kang, G. Gao, H.S. Kang, J. Ko, Inorg. Chem. 49 (2010) 8351.

[55] H. Choi, C. Baik, S. Kim, M.-S. Kang, X. Xu, H.S. Kang, S.O. Kang, J. Ko, M.K. Nazeeruddin, M. Grätzel, New J. Chem. 32 (2008) 2233.

[56] C.-Y. Chen, J.-G. Chen, S.-J. Wu, J.-Y. Li, C.-G. Wu, K.-C. Ho, Angew. Chem. Int. Ed. 47 (2008) 7342.

[57] C.-Y. Chen, N. Pootrakulchote, S.-J. Wu, M. Wang, J.-Y. Li, J.-H. Tsai, C.-G. Wu, S.M. Zakeeruddin, M. Grätzel, J. Phys. Chem. C 113 (2009) 20752.

[58] J.-Y. Li, C.-Y. Chen, J.-G. Chen, C.-J. Tan, K.-M. Lee, S.-J. Wu, Y.-L. Tung, H.-H. Tsai, K.-C. Ho, C.-G. Wu, J. Mater. Chem. 20 (2010) 7158.

[59] N. Onozawa-Komatsuzaki, O. Kitao, M. Yanagida, Y. Himeda, H. Sugihara, K. Kasuga, New J. Chem. 30 (2006) 689.

[60] A. Reynal, A. Forneli, E. Martinez-Ferrero, A. Sánchez-Díaz, A. Vidal-Ferran, E. Palomares, Eur. J. Inorg. Chem. (2008) 1955.

[61] A. Reynal, A. Forneli, E. Martinez-Ferrero, A. Sánchez-Díaz, A. Vidal-Ferran, B.C. O'Regan, E. Palomares, J. Am. Chem. Soc. 130 (2008) 13558.

[62] C.-Y. Chen, H.-C. Lu, C.-G. Wu, J.-G. Chen, K.-C. Ho, Adv. Funct. Mater. 17 (2007) 29.

[63] X.H. Li, J. Gui, H. Yang, W.J. Wu, F.Y. Li, H. Tian, C.H. Huang, Inorg. Chim. Acta 361 (2008) 2835.

[64] J.-F. Yin, D. Bhattacharya, Y.-C. Hsu, C.-C. Tsai, K.-L. Lu, H.-C. Lin, J.-G. Chen, K.-C. Ho, J. Mater. Chem. 19 (2009) 7036.

[65] J.-F. Yin, J.-G. Chen, Z.-Z. Lu, K.-C. Ho, H.-C. Lin, K.-L. Lu, Chem. Mater. 22 (2010) 4392.

[66] J.-F. Yin, J.-G. Chen, J.-T. Lin, D. Bhattacharya, Y.-C. Hsu, H.-C. Lin, K.-C. Ho, K.-L. Lu, J. Mater. Chem. 22 (2012) 130.

[67] S.-H. Fan, A.-G. Zhang, C.-C. Ju, L.-H. Gao, K.-Z. Wang, Inorg. Chem. 49 (2010) 3752.

[68] P. Wang, R. Humphry-Baker, J.-E. Moser, S.M. Zakeeruddin, M. Grätzel, Chem. Mater. 16 (2004) 3246.

[69] Z. Jin, H. Masuda, N. Yamanaka, M. Minami, T. Nakamura, Y. Nishikitani, J. Phys. Chem. C 113 (2009) 2618.

[70] J.-J. Kim, H. Choi, C. Kim, M.-S. Kang, H.S. Kang, J. Ko, Chem. Mater. 21 (2009) 5719.

[71] M. Yanagida, L.P. Singh, K. Sayama, K. Hara, R. Katoh, A. Islam, H. Sugihara, H. Arakawa, M.K. Nazeeruddin, M. Gratzel, J. Chem. Soc. Dalton Trans. (2000) 2817.

[72] A. Islam, H. Sugihara, L.P. Singh, K. Hara, R. Katoh, Y. Nagawa, M. Yanagida, Y. Takahashi, S. Murata, H. Arakawa, Inorg. Chim. Acta 322 (2001) 7.

[73] Y.-C. Hsu, H. Zheng, J.T. Lin, K.-C. Ho, Sol. Energy Mater. Sol. Cells 87 (2005) 357.

[74] C. Klein, M.K. Nazeeruddin, P. Liska, D. Di Censo, N. Hirata, E. Palomares, J.R. Durrant, M. Grätzel, Inorg. Chem. 44 (2005) 178.

[75] A. Mishra, N. Pootrakulchote, M.K.R. Fischer, C. Klein, M.K. Nazeeruddin, S.M. Zakeeruddin, P. Bäuerle, M. Grätzel, Chem. Commun. (2009) 7146.

[76] A. Mishra, N. Pootrakulchote, M. Wang, S.-J. Moon, S.M. Zakeeruddin, M. Grätzel, P. Bäuerle, Adv. Func. Mater. 21 (2011) 963.

[77] K.-S. Chen, W.-H. Liu, Y.-H. Wang, C.-H. Lai, P.-T. Chou, G.-H. Lee, K. Chen, H.-Y. Chen, Y. Chi, F.-C. Tung, Adv. Funct. Mater. 17 (2007) 2964.

[78] K. Chen, Y.-H. Hong, Y. Chi, W.-H. Liu, B.-S. Chen, P.-T. Chou, J. Mater. Chem. 19 (2009) 5329.

[79] B.-S. Chen, K. Chen, Y.-H. Hong, W.-H. Liu, T.-H. Li, C.-H. Lai, P.-T. Chou, Y. Chi, G.-H. Lee, Chem. Commun. (2009) 5844.

[80] S.-H. Yang, K.-L. Wu, Y. Chi, Y.-M. Cheng, P.-T. Chou, Angew. Chem. Int. Ed. 50 (2011) 8270.

[81] S.M. Zakeeruddin, M.K. Nazeeruddin, R. Humphry-Baker, M. Grätzel, V. Shklover, Inorg. Chem. 37 (1998) 5251.

[82] T. Bessho, E. Yoneda, J.-H. Yum, M. Guglielmi, I. Tavernelli, H. Imai, U. Rothlisberger, M.K. Nazeeruddin, M. Grätzel, J. Am. Chem. Soc. 131 (2009) 5930.

[83] K.-L. Wu, H.-C. Hsu, K. Chen, Y. Chi, M.-W. Chung, W.-H. Liu, P.-T. Chou, Chem. Commun. 46 (2010) 5124.

[84] C.-C. Chou, K.-L. Wu, Y. Chi, W.-P. Hu, S.J. Yu, G.-H. Lee, C.-L. Lin, P.-T. Chou, Angew. Chem. Int. Ed. 50 (2011) 2054.

[85] S.H. Wadman, J.M. Kroon, K. Bakker, R.W.A. Havenith, G.P.M. van Klink, G. van Koten, Organometallics 29 (2010) 1569.

[86] K.C.D. Robson, B.D. Koivisto, A. Yella, B. Sporinova, M.K. Nazeeruddin, T. Baumgartner, M. Grätzel, C.P. Berlinguette, Inorg. Chem. 50 (2011) 5494.

[87] K.C.D. Robson, B. Sporinova, B.D. Koivisto, E. Schott, D.G. Brown, C.P. Berlinguette, Inorg. Chem. 50 (2011) 6019.

[88] B.D. Koivisto, K.C.D. Robson, C.P. Berlinguette, Inorg. Chem. 48 (2009) 9644.

[89] M.K. Nazeeruddin, P. Péchy, M. Grätzel, J. Chem. Soc. Chem. Commun. (1997) 1705.

[90] M.K. Nazeeruddin, S.M. Zakeeruddin, R. Humphry-Baker, S.I. Gorelsky, A.B.P. Lever, M. Grätzel, Coord. Chem. Rev. 208 (2000) 213.

[91] C. Barolo, M.K. Nazeeruddin, S. Fantacci, D. Di Censo, P. Comte, P. Liska, G. Viscardi, P. Quagliotto, F. De Angelis, S. Ito, M. Grätzel, Inorg. Chem. 45 (2006) 4642.

[92] A. Abbotto, F. Sauvage, C. Barolo, F. De Angelis, S. Fantacci, M. Graetzel, N. Manfredi, C. Marinzi, M.K. Nazeeruddin, Dalton Trans. 40 (2011) 234.

[93] W.-K. Huang, C.-W. Cheng, S.-M. Chang, Y.-P. Lee, E.W.-G. Diau, Chem. Commun. 46 (2010) 8992.

[94] I. Stengel, A. Mishra, N. Pootrakulchote, S.-J. Moon, S.M. Zakeeruddin, M. Grätzel, P. Bäuerle, J. Mater. Chem. 21 (2011) 3726.

[95] S. Ferrere, B.A. Gregg, J. Am. Chem. Soc. 120 (1998) 843.

[96] E.A.M. Geary, N. Hirata, J. Clifford, J.R. Durrant, S. Parsons, A. Dawson, L.J. Yellowlees, N. Robertson, Dalton Trans. (2003) 3757.

[97] J.B. Asbury, E.C. Hao, Y.Q. Wang, T.Q. Lian, J. Phys. Chem. B 104 (2000) 11957.

[98] E.I. Mayo, K. Kilså, T. Tirrell, P.I. Djurovich, A. Tamayo, M.E. Thompson, N.S. Lewis, H.B. Gray, Photochem. Photobiol. Sci. 5 (2006) 871.

[99] A. Yella, H.-W. Lee, H.N. Tsao, C. Yi, A.K. Chandiran, M.K. Nazeeruddin, E.W.-G. Diau, C.-Y. Yeh, S.M. Zakeeruddin, M. Grätzel, Science 334 (2011) 629.

[100] B.E. Hardin, H.J. Snaith, M.D. McGehee, Nat. Photon. 6 (2012) 162.